APPLIED SCIENCES AND ENGINEERING

Macrophage-targeted *Mms6* mRNA-lipid nanoparticles promote locomotor functional recovery after traumatic spinal cord injury in mice

Chunyan Fu[1]†, Xiaoqin Jin[2]†, Kangfan Ji[3]†, Ke Lan[4], Xingjia Mao[5], Zhaobo Huang[6], Jian Chen[6], Fengdong Zhao[6], Pengfei Li[7], Xuefei Hu[7], Liwen Sun[7], Ning Lu[7], Jinjie Zhong[5]*, Yingying Chen[8]*, Linlin Wang[1,7]*

Traumatic spinal cord injury (SCI) causes severe central nervous system damage. M2 macrophages within the lesion are crucial for SCI recovery. Our previous research revealed that M2 macrophages transfected with magnetotactic bacteria–derived *Mms6* gene can resist ferroptosis and enhance SCI recovery. To address the limitations of M2 macrophage transplantation, we developed lipid nanoparticles (LNPs) encapsulating *Mms6* mRNA targeting macrophages (*Mms6* mRNA-PS/LNPs). The targeting efficiency and therapeutic effect of these LNPs in SCI mice were evaluated. Intravenous administration of *Mms6* mRNA-PS/LNPs delivered more *Mms6* mRNAs to lesion-site macrophages than those in the *Mms6* mRNA-LNP group, which resulted in enhancing motor function recovery, reducing lesion area and scar formation, and promoting neuronal survival and nerve fiber repair. These effects were nullified when macrophages were depleted. These findings suggest that macrophage-targeted delivery of *Mms6* mRNA is a promising therapeutic strategy for promoting spinal cord repair and motor function recovery in patients with traumatic SCI.

INTRODUCTION

Traumatic spinal cord injury (SCI) severely damages the central nervous system, causing severe neurological deficits and long-term disabilities (*1*). SCI was once thought to have no way of reducing its neurological deficits (*2*). However, recently, neurorestorative treatments have partially restored the damaged neurological functions of this injury (*3*). Research indicates that the immune system (*4*), particularly M2 macrophages, plays a pivotal role in SCI recovery by clearing debris and releasing anti-inflammatory mediators soon after injury (*5*).

Enhancing these macrophages' abilities through genetic modification provides a promising method for improving recovery outcomes following SCI (*4*). Since the 1970s, mRNA-based therapies have been developed to induce overexpression of target proteins in cells and have demonstrated considerable potential in cell-based treatments (*6*, *7*). MMS6 protein, which is exclusively expressed in magnetotactic bacteria, has a powerful property of iron capture and storage via the synthesis of magnetic nanoparticles (*8*). Our previous study has suggested that transfection of macrophages with *Mms6* gene, which was known to strengthen macrophage phagocytic function and confer resistance to ferroptosis (an iron-dependent form of regulated cell death characterized by lipid peroxidation), seems to be a potent tool for therapeutic intervention (*9*). However, the employment of autologous M2 macrophage transplantation in clinical settings has been reported to be hindered by complex procedures and potential immune reactions.

Recent studies have implied that transporting mRNA directly to the endogenous cells within the body using a lipid nanoparticle (LNP)–based delivery system is a more feasible alternative. This idea is grounded in the proven track record of LNPs in the successful development of mRNA-based COVID-19 vaccines, which demonstrates that the LNP delivery platform is safe and effective (*10*). Considering the potentiality of the LNP-based delivery platform, LNPs containing *Mms6* mRNA (*Mms6* mRNA-LNPs) were constructed and administrated to SCI mice by intravenous or intraperitoneal injection in the present study, and then their effect on locomotor functional recovery after SCI was explored. Because the blood–spinal cord barrier after SCI is commonly disrupted (*11*), the small molecular or some immune cells in the peripheral bloodstream would normally be triggered to get into the injured spinal cord and help repair the damage (*4*, *12*). We speculated that the intravenously or intraperitoneally injected *Mms6* mRNA-LNPs could also easily pass through the blood–spinal cord barrier and then be engulfed by resident or infiltrating macrophages in the injured spinal cord to enhance their repair ability.

However, the mRNA-loaded LNPs in the bloodstream can arrive in many different tissues and be endocytosed by various types of cells, resulting in only a small number of them reaching the target tissues or cells. To solve this problem, some cell-targeting antibodies have been designed and decorated on the LNP surface (*13*–*15*). In the present study, the construction of macrophage-targeted LNPs was a prerequisite for making sure that LNPs were mainly delivered to the macrophages and sufficient *Mms6* mRNA would be expressed in macrophages, which leads to effectively improving the functional therapeutic effect in SCI mice in vivo. Phosphatidylserine (PS) has been reported as a recognition signal for macrophages (*16*). PS is

[1]Department of Orthopaedics of Sir Run Run Shaw Hospital and Department of Basic Medicine Sciences, Zhejiang University School of Medicine, Hangzhou 310016, PR China. [2]Academy of Chinese Medical Sciences, Zhejiang Chinese Medical University, Hangzhou 310053, PR China. [3]State Key Laboratory of Advanced Drug Delivery and Release Systems, College of Pharmaceutical Sciences, Zhejiang University, Hangzhou 310058, PR China. [4]Department of Medical Stomatology, Zhejiang University School of Medicine, Hangzhou 310058, PR China. [5]Department of Basic Medicine Sciences, Zhejiang University School of Medicine, Hangzhou 310058, PR China. [6]Department of Orthopaedics of Sir Run Run Shaw Hospital, Zhejiang University School of Medicine, Hangzhou 310058, PR China. [7]Tarim University School of Medicine, Alaer 843300, PR China. [8]Department of Obstetrics of the Second Affiliated Hospital and Department of Basic Medicine Sciences, Zhejiang University School of Medicine, Hangzhou 310009, PR China.
*Corresponding author. Email: 0017152@zju.edu.cn (J.Z.); bchenyy@zju.edu.cn (Y.C.); wanglinlin@zju.edu.cn (L.W.)
†These authors contributed equally to this work.

recognized by macrophage surface receptors, including Tim4, BAI1, and Stabilin-2, which mediate efferocytosis and other processes linked to macrophage activation and function (*17*). We hypothesized that incorporating PS on the surface of LNPs would increase the macrophage-targeted delivery of *Mms6* mRNA and enhance the therapeutic effects, minimizing the risk of side effects caused by nonspecific delivery.

The present study aimed to engineer *Mms6* mRNA-loaded LNPs for targeted delivery to macrophages and investigate whether these LNPs could promote locomotor functional recovery following SCI by enhancing the anti-ferroptosis of macrophages. Compared with traditional cell-based therapies, the innovative approach used in this study might be a promising non-genotoxic alternative for treating SCI. This study might also widen potential applications of gene-modified therapeutic strategies for treating various neurological conditions.

RESULTS

Characteristics of *Mms6* mRNA-LNPs and their role in alleviating macrophage ferroptosis in vitro

To explore the therapeutic potential of *Mms6* mRNA-LNPs in SCI mice, *Mms6* mRNA, a potent gene against ferroptosis (*9*), was encapsulated into LNPs (Fig. 1A). These mRNA-containing LNPs were characterized to have an average size of 107.03 nm, a zeta potential of −3.678 mV, a polydispersity index (PDI) of 0.123, and an encapsulation efficiency of ~94.30%, ensuring their potential for robust delivery (Fig. 1B). The uniform size distribution was further validated using cryo–electron microscopy (cryo-EM), confirming the successful formulation of the nanoparticles (Fig. 1C). The transfection efficiency of *Mms6* mRNA-LNPs into macrophages, measured by using enhanced green fluorescent protein (eGFP)– and mCherry-labeled techniques, is ~95% (Fig. 1D).

Next, the functional analysis of macrophages was assessed using Prussian blue staining and transmission electron microscopy. A significantly higher accumulation of nontoxic, trivalent iron (Fig. 1E) was found in *Mms6* mRNA-LNP–transfected macrophages after being treated with ferric quinate. The trivalent iron within these macrophage cytoplasm was present in the form of high-density spherical magnetic nanoparticles (~10 to 20 nm in diameter), which gathered in ring or long-chain arrangements (Fig. 1F), while no magnetic nanoparticles were visible in the macrophages transfected with empty LNPs (fig. S1). These results suggested that macrophages transfected with *Mms6* mRNA-LNPs exhibited a greater ability of iron capture and storage.

Then, the protective effect of *Mms6* mRNA-LNPs against ferroptosis under hypoxic injury was evaluated in the in vitro–cultured macrophages. Macrophages were treated with cobalt chloride ($CoCl_2$) to mimic the hypoxic condition of post-SCI. The results found that the intercellular levels of Fe^{2+} and lipid peroxidation were considerably lower in *Mms6* mRNA-LNP–transfected macrophages than those of empty LNP–treated macrophages (Fig. 1, H to K), indicating that transfection with *Mms6* mRNA-LNPs could effectively alleviate hypoxia-induced ferroptosis in macrophages. These in vitro experiments demonstrated the effectiveness of *Mms6* mRNA-LNPs in improving the anti-ferroptosis capabilities of macrophages via managing the balance of cellular iron metabolism in a hypoxic condition, which is common in SCI.

Furthermore, the neuroprotective effect of *Mms6* mRNA-LNP–transfected macrophages in an in vitro hypoxia environment was further investigated. $CoCl_2$ (400 μM)–induced hypoxic injury model of NSC-34 motor neuron–like cells was used to mimic the SCI environment according to our previous study (*9*). As shown in Fig. 1G, after incubation with $CoCl_2$ for 24 hours, NSC-34 cells cocultured with *Mms6* mRNA-LNP–treated macrophages had a significantly lower percentage of cell death than those cocultured with empty LNPs ($P < 0.01$). These findings further validated that *Mms6* mRNA-LNP–treated macrophages might have the potential to rescue neuronal cells in the SCI microenvironment through the formation of magnetic bio-nanoparticles.

Intravenous injection of LNPs delivered mRNA more efficiently to the injured spinal cord compared with intraperitoneal administration

To investigate the efficacy of nonviral mRNA-loaded LNP delivery systems in vivo, LNPs encapsulated with firefly luciferase mRNA (FLuc mRNA) were administrated to SCI mice via intravenous or intraperitoneal injection at a dosage of 0.5 mg/kg. The distribution of LNPs in mice was monitored at 3 to 120 hours after the injection using a bioluminescence imaging technique. A significantly higher and more sustained luminescent signal was detected in the injured spinal cord of mice receiving intravenous administration of FLuc mRNA-LNPs compared with that of the intraperitoneal injection group (Fig. 2, A and B). The data showed that luminescent signals in the injured spinal cord reached the peak at 9 hours after intravenous injection, which was 10-fold the spike of luminescent signals that occurred at 9 hours postinjection in the intraperitoneal administration group (Fig. 2, A and B), so the injured spinal cords at 9 hours after intravenous injection were collected for the further study. These results indicated that the intravenous route had a more efficient delivery of mRNA to the injured spinal cord than that of intraperitoneal injection.

Although mRNA-containing LNPs injected via intravenous route could get into the injured spinal cord, it was more important to clarify that these LNPs would be mainly taken in by what kind of cells. This is because different types of cells within the lesion have their distinctive roles during SCI repair, precisely targeted intervention to specific cell types in damaged tissues might help achieve optimal therapeutic efficacy (*18*, *19*). After mCherry-labeled *Mms6* mRNA-LNPs were injected into SCI mice, selective cellular uptake of LNPs was analyzed. After 9 hours postinjection, mRNA-containing LNPs were mainly visible within macrophages (tissue-resident and infiltrated macrophages) and neurons, while these LNPs were hardly detected in endothelial cells or astrocytes (Fig. 2C).

Furthermore, the mRNA-LNP uptake capacities of macrophage populations in the injured spinal cord were assessed using flow cytometry. After injection of LNPs encapsulated eGFP-labeled *Mms6* mRNA, total infiltrated macrophages (Mφ) and their subtypes were detected by $F4/80^{+}CD45^{high}$, $F4/80^{+}CD45^{high}CD86^{+}$, and $F4/80^{+}CD45^{high}CD206^{+}$, respectively (fig. S2 and table S1). The data showed that the number of total Mφ and their subtypes (M1φ and M2φ) in the injured spinal cord did not change (Fig. 2D). However, about 7% of total macrophages were transfected by eGFP-*Mms6* mRNA-LNPs, and the enhanced uptake percentage of mRNA-containing LNPs between M1- and M2-type macrophages was not significantly different (Fig. 2E, fig. S2, and table S1). The results also revealed that microglia, the tissue-resident macrophages in the central nervous system, might have the similar phagocytosis property and could engulf mRNA-loaded LNPs (Fig. 2F, fig. S2, and table S1).

These findings demonstrated that intravenous injection of mRNA-containing LNPs is a feasible and convenient alternative

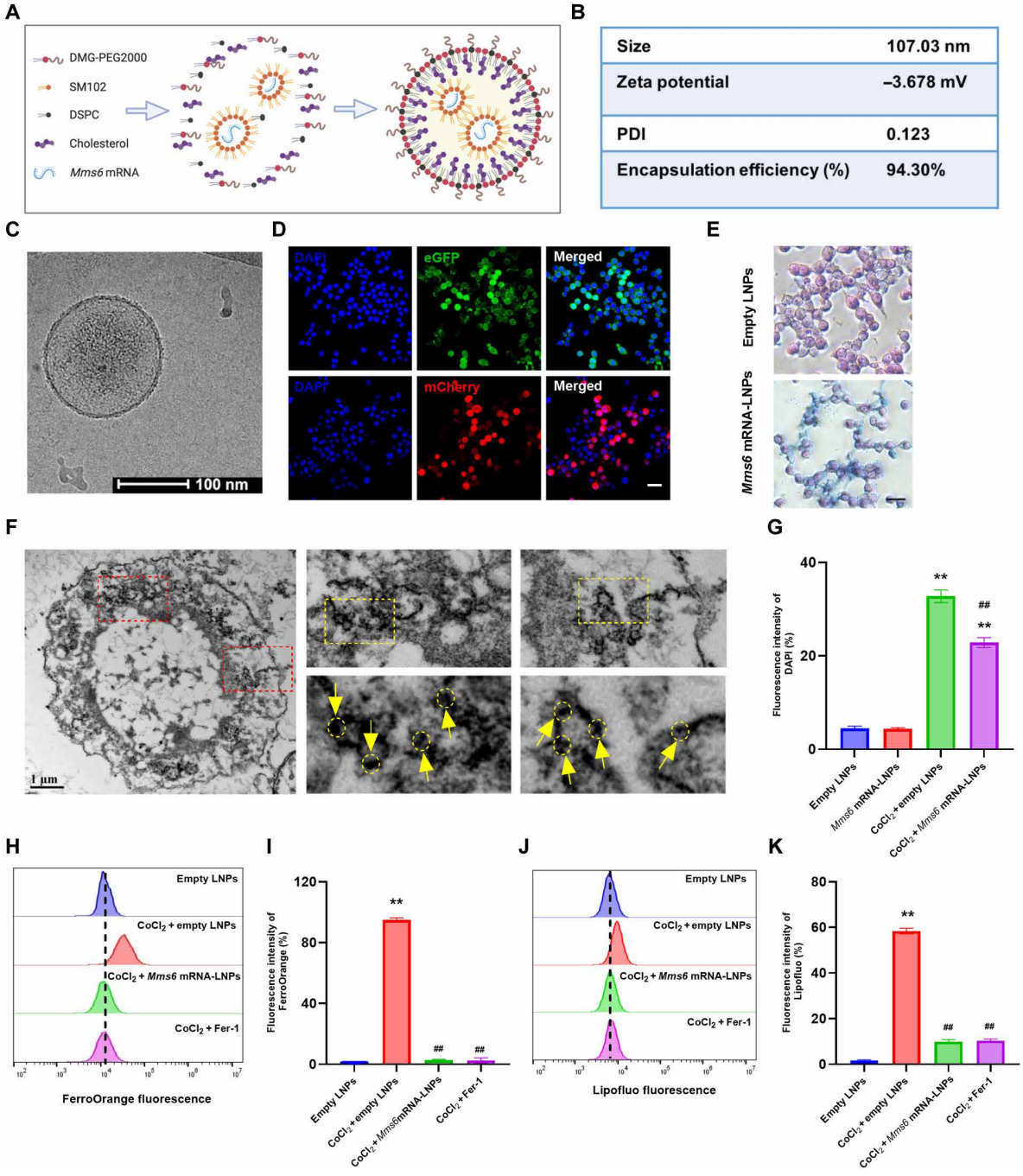

Fig. 1. Evaluation of characteristics and anti-ferroptosis properties of *Mms6* mRNA-LNPs. (**A**) Schematic illustration of *Mms6* mRNA-LNP formulation. SM102, an ionizable lipid crucial for forming stable lipid nanoparticles and facilitating the endosomal escape from the encapsulated material; DSPC, a phospholipid, enhances nanoparticle stability and delivery; cholesterol, maintains integrity and rigidity of outer lipid bilayer; DMG-PEG2000, a polyethylene glycol (PEG) lipid enhances nanoparticle stability and prolongs circulation time by reducing aggregation and immune recognition; *Mms6* mRNA, encodes MMS6 protein to resist ferroptosis. (**B**) Measurement of particle size, zeta potential, polydispersity index (PDI), and encapsulation efficiency of *Mms6* mRNA-LNPs. (**C**) Representative cryo–electron microscopy (cryo-EM) image of *Mms6* mRNA-LNPs. (**D**) Representative eGFP fluorescence (green)–labeled or mCherry fluorescence (red)–labeled *Mms6* mRNA-LNPs in macrophages. Cell nuclei were stained with DAPI (blue). Scale bar, 40 μm. (**E**) Prussian blue stain detecting storage form of ferric iron in macrophages. Scale bar, 50 μm. (**F**) Representative transmission electron microscopy images showing the formation of magnetic nanoparticles in *Mms6* mRNA-LNP–transfected macrophages (scale bar, 1 μm). (**G**) NSC-34 cells, which cocultured with macrophages transfected with either *Mms6* mRAN-LNPs or empty LNPs, were incubated with or without $CoCl_2$ (400 μM, a chemical hypoxia mimetic agent) for 24 hours. Then, the mean fluorescence intensity of DAPI in NSC-34 cells was measured ($n = 6$). $^{**}P < 0.01$ versus empty LNP group; $^{\#\#}P < 0.01$ versus $CoCl_2$ + empty LNP group. (**H** and **J**) Macrophages, transfected with *Mms6* mRAN-LNPs or empty LNPs, were treated with $CoCl_2$ and/or Fer-1 (ferrostatin-1, an inhibitor of ferroptosis) for 24 hours. Representative images of free Fe^{2+} (FerroOrange staining) and lipid peroxidation (Lipofluo staining) using flow cytometry. (**I** and **K**) Statistical analysis of the mean fluorescence intensity of FerroOrange and Lipofluo ($n = 3$). $^{**}P < 0.01$ versus empty LNP group; $^{\#\#}P < 0.01$ versus $CoCl_2$ + empty LNP group.

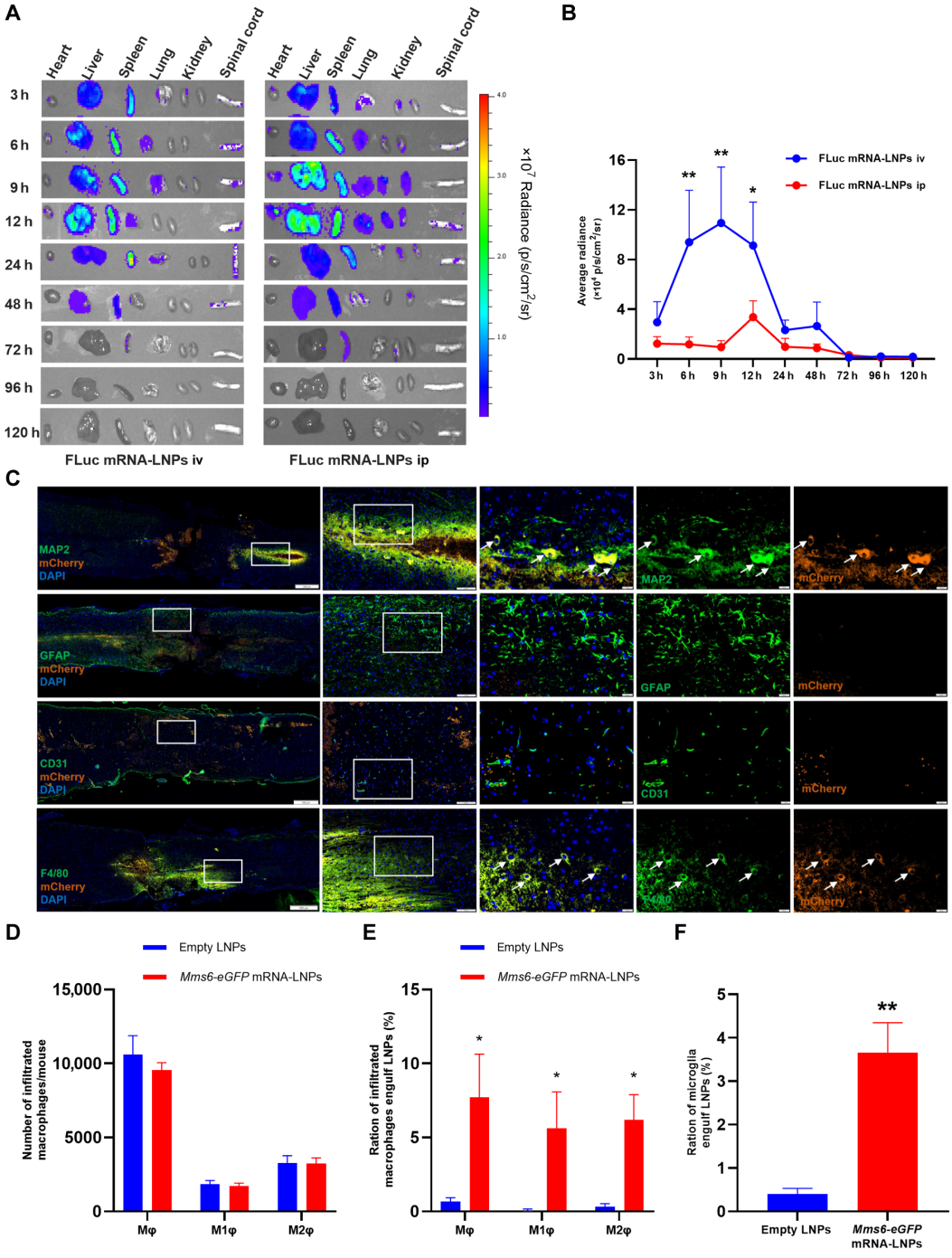

Fig. 2. Intravenous administration of LNPs delivered mRNA more efficiently to the injured spinal cord compared with intraperitoneal injection. (**A**) Representative in vivo imaging system images of major organs in SCI mice after being administered with firefly luciferase (FLuc) mRNA-LNPs (0.5 mg mRNA/kg). From left to right are the heart, liver, spleen, lung, two kidneys, and spinal cord. iv, intravenous; ip, intraperitoneal. (**B**) Quantification of FLuc expression in the injured spinal cord ($n = 3$ mice per group). $^{*}P < 0.05$ and $^{**}P < 0.01$ versus FLuc mRNA-LNP intraperitoneal group. (**C**) Immunofluorescence analyzing the cellular distribution of *Mms6* mRNA-LNPs in the injured spinal cord. *Mms6* mRNAs in LNPs were labeled with mCherry (orange). Neurons, astroglia, endothelial cells, and tissue-resident and infiltrated macrophages were detected by their markers [microtubule-associated protein 2 (MAP2), glial fibrillary acidic protein (GFAP), CD31, or F4/80, respectively] (green). White arrows pinpoint the cells in which MAP2 or F4/80 co-localizes with mCherry. The mCherry fluorescence was not visible in GFAP or CD31-positive cells. Scale bars, 20 μm. (**D**) Statistical analysis of flow cytometry results showing numbers of total infiltrated macrophages (Mφ) and their subtypes (M1φ and M2φ) in the injured spinal cord after intravenous injection of *Mms6-eGFP* mRNA-LNPs ($n = 5$). (**E**) Statistical analysis of flow cytometry results showing the percentage of macrophages containing eGFP-labeled *Mms6* in the injured spinal cord of mice that received intravenous administration of *Mms6*-eGFP mRNA-LNPs ($n = 6$). $^{*}P < 0.05$ versus empty LNP group. (**F**) Statistical analysis of flow cytometry results showing the percentage of microglia (tissue-resident macrophages) containing eGFP-labeled *Mms6* in the injured spinal cord that received intravenous administration of *Mms6-eGFP* mRNA-LNPs ($n = 5$). $^{**}P < 0.01$ versus empty LNP group. h, hours.

for delivering mRNA directly to the specific cell types in the injured spinal cord following SCI. This method not only reduces the risks associated with more invasive delivery techniques like intrathecal injection but also makes the therapeutic agents delivered more efficiently into specific cells, which is crucial to SCI repair.

Intravenous injection of *Mms6* mRNA-LNPs promoted locomotor function recovery and morphological repair in traumatic SCI mice

The effects of *Mms6* mRNA-LNPs on locomotor functional recovery and morphological repair of the injured spinal cord were evaluated in a mouse SCI model (Fig. 3A and fig. S3A).

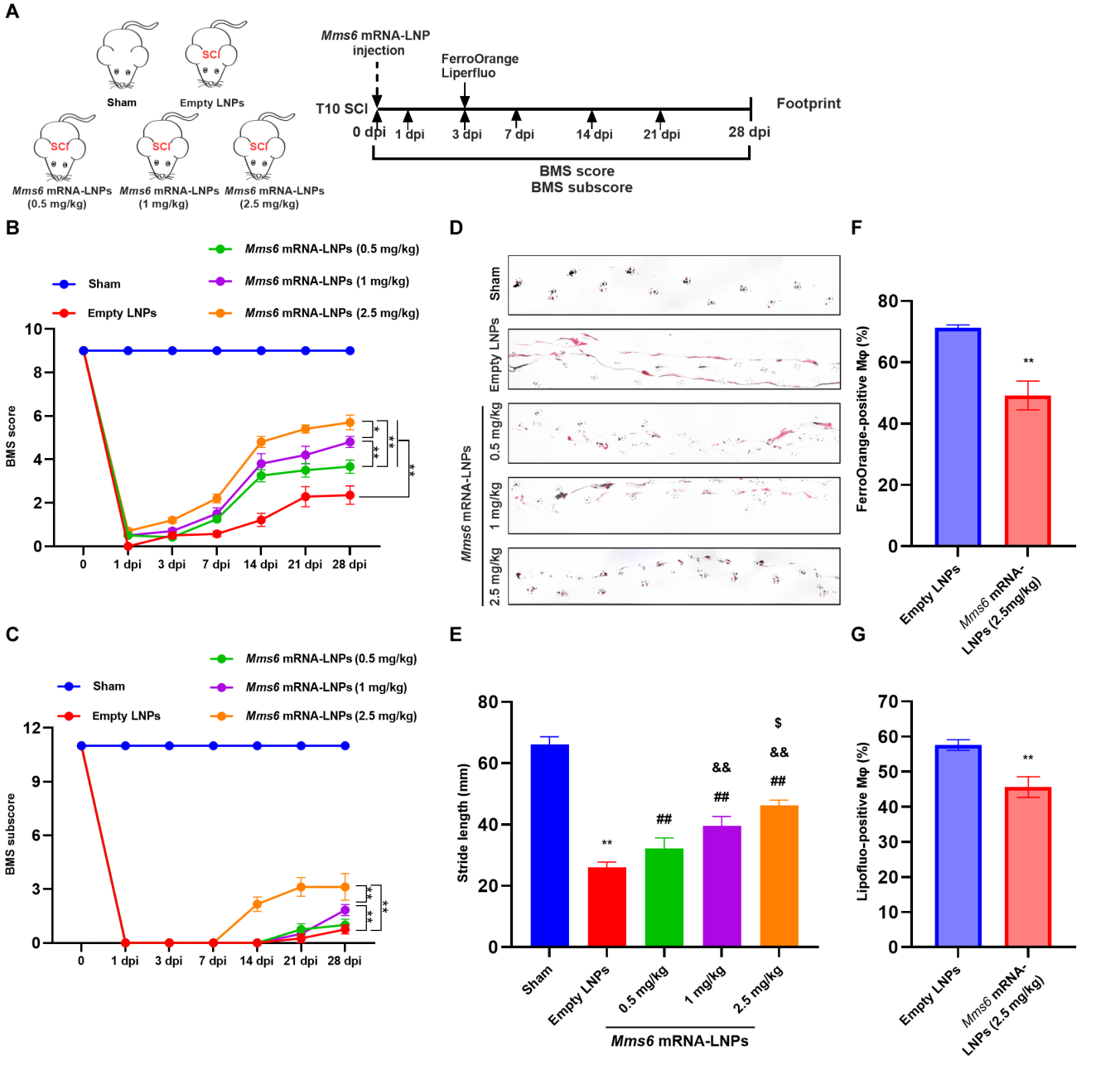

Fig. 3. Intravenous injection of *Mms6* mRNA-LNPs promoted locomotor function recovery and inhibited Mφ ferroptosis in traumatic SCI. (**A**) Schematics of the experimental workflow. SCI mice were received a single injection of *Mms6* mRNA-LNPs. (**B** and **C**) Basso Mouse Scale (BMS) scores and subscores were assessed in SCI mice ($n = 6$ mice per group). *$P < 0.05$ and **$P < 0.01$. (**D**) Representative footprint images at 28 dpi of SCI. The forelimbs and hindlimbs were painted in black and red, respectively. (**E**) Evaluation of stride length using footprint images ($n = 6$ mice per group). **$P < 0.01$ versus Sham group; ##$P < 0.01$ versus empty LNP group; &&$P < 0.01$ versus *Mms6* mRNA-LNP (0.5 mg/kg) group; \$$P < 0.05$ versus *Mms6* mRNA-LNP (1 mg/kg) group. (**F**) Statistical analysis of flow cytometry results showing the percentage of FerroOrange positive Mφ ($n = 3$ mice per group). **$P < 0.01$ versus empty LNP group. (**G**) Statistical analysis of flow cytometry results showing the percentage of Liperfluo positive Mφ ($n = 3$ mice per group). **$P < 0.01$ versus empty LNP group. dpi, days post-injury.

The recovery of motor function in SCI mice was assessed using standardized behavioral tests, including Basso Mouse Scale (BMS) and footprint analysis (*9*, *20*). Intravenous injection of *Mms6* mRNA-LNPs (0.5, 1, or 2.5 mg/kg) immediately after SCI could remarkably increase BMS score and subscore, enhance stride length, and mitigate the hindlimb dragging in a dose-dependent manner (Fig. 3, B to E). Our results indicated there was no significant difference in function recovery of SCI mice between the phosphate-buffered saline (PBS) + SCI and empty LNP + SCI groups ($P > 0.05$; fig. S4). Compared with the mice receiving a single injection of *Mms6* mRNA-LNPs (0.5 mg/kg) immediately after SCI, the BMS score, BMS subscore, and stride length were not significantly increased in SCI mice being given multiple injections at the same dose (fig. S3, B to E).

Next, morphological changes in the injured spinal cord were further checked at 28 days post-injury (dpi) of SCI in mice receiving a single injection of *Mms6* mRNA-LNPs (0.5, 1, or 2.5 mg/kg) (Fig. 4A). Hematoxylin and eosin (H&E) staining results showed a disrupted cellular architecture in the injured spinal cord characterized by disordered cell alignment in mice following SCI (Fig. 4B). Notably, intravenous administration of *Mms6* mRNA-LNPs significantly decreased lesion areas in SCI mice (Fig. 4, B and C). Results of Masson's trichrome and Nissl staining also displayed that intravenous administration of *Mms6* mRNA-LNPs reduced scar formation and increased neuronal survival in the injured spinal cords (Fig. 4, B, D, and E). Additionally, nerve fiber repair was assayed using microtubule-associated protein 2 (MAP2) staining. The data revealed that, compared with the empty LNP group, injection of *Mms6* mRNA-LNPs significantly increased nerve fiber repair in SCI mice (Fig. 4, F and G). Our results indicated that there was no significant difference in morphological repair of the injured spinal cord between the PBS + SCI and empty LNP + SCI groups ($P > 0.05$; fig. S5). Compared with the mice receiving a single injection of *Mms6* mRNA-LNPs (0.5 mg/kg) immediately after SCI, the H&E, Masson's trichrome, and Nissl staining and nerve fiber repair were not significantly increased in SCI mice being given multiple injections at the same dose (fig. S4, A to F). These findings suggested that intravenous injection of *Mms6* mRNA-LNPs promoted both morphological repair and functional recovery of the injured spinal cord in a dose-dependent manner.

Furthermore, results of H&E staining and biochemical assessments indicated that injection of *Mms6* mRNA-LNPs (2.5 mg/kg) had no substantial toxic effects on the heart, liver, spleen, and kidney (fig. S6), suggesting that the administration route and the dose of *Mms6* mRNA-LNPs used in this experiment were safe. Therefore, *Mms6* mRNA-LNPs at a dose of 2.5 mg/kg were selected for subsequent experiments.

Depletion of macrophages abolished *Mms6* mRNA-LNP–induced promotion of morphological repair and functional recovery after SCI

Considering the fact that macrophages play a crucial role in SCI recovery and the above results showing that *Mms6* mRNA-containing LNPs, after entering the injured spinal cord, were mainly engulfed by the macrophages, the properties, and the role of macrophages in the injured spinal cord after injection of *Mms6* mRNA-LNPs were further explored. First, after administration of *Mms6* mRNA-LNPs, whether the macrophages at the injured spinal cord also obtained an enhanced ability against ferroptosis, as those in in vitro experiments, was investigated. At 3 days after injection of *Mms6* mRNA-LNPs (2.5 mg/kg), the macrophages in the injured spinal cords were sorted, and the intracellular Fe^{2+} and lipid peroxidation levels were measured using flow cytometric analysis. The results showed that macrophage ferroptosis in the *Mms6* mRNA-LNP–treated SCI mice was significantly decreased, as evidenced by lower levels of intracellular Fe^{2+} and lipid peroxidation when compared with that in the empty LNP group (Fig. 3, F and G). These observations confirmed that *Mms6* mRNA-LNPs can effectively help macrophages to counteract ferroptosis in vivo, mirroring the protective effects in our in vitro studies.

Second, clodronate-liposomes (Clodrosome), a macrophage-depleting agent, were used to elucidate the indispensable role of macrophages in the *Mms6* mRNA-LNP–induced protective effect in mice after SCI. Clodrosome has been recognized for its effectiveness in the depletion of endogenous macrophages in experimental animals (*21*, *22*). The immunohistochemistry and flow cytometric analysis results showed that, after C57BL/6J mice were injected with Clodrosome, substantial depletion of macrophages was achieved at 48 hours after injection (fig. S7). After macrophages being depleted, mice were suffered from SCI and received an intravenous administration of *Mms6* mRNA-LNPs (2.5 mg/kg). The beneficial effects of *Mms6* mRNA-LNP treatment on the promotion of function recovery and morphology repair were significantly abolished in macrophage-depleting SCI mice (Figs. 5 and 6), suggesting the essential role of macrophages in mediating the therapeutic effects of *Mms6* mRNA-LNPs.

Synthesis of macrophage-targeted *Mms6* mRNA-PS/LNPs and the delivery of mRNA to the injured spinal cord

Although LNPs could deliver *Mms6* mRNA to the macrophages, *Mms6* mRNA-loaded LNPs would also be engulfed by other cells. To increase the macrophage-targeted mRNA delivery efficiency of LNPs, an LNP delivery system containing PS on the surface was developed in the present study (Fig. 7A). The PS/LNP delivery system is based on the propriety of PS, which as a membrane molecule, can be recognized by macrophages (*23*). It has been reported that PS/LNPs also leverage the PS-specific receptor Tim4 on macrophages to enhance endocytic activity and efficacy (*24*). The physical properties of *Mms6* mRNA-PS/LNPs, synthesized in our study, were characterized to have an average size of 176.3 nm, zeta potential of −6.2 mV, a PDI of 0.116, and an encapsulation efficiency of ~87.63% (Fig. 7, B and C).

Then, cultured macrophages were exposed to *Mms6* mRNA-PS/LNPs. The transfection efficiency of *Mms6* mRNA-PS/LNPs into macrophages is ~99% (Fig. 7D), which was similar to that of macrophages treated with *Mms6* mRNA-LNPs. Prussian blue staining and electron microscopy demonstrated that macrophages incubated with *Mms6* mRNA-PS/LNPs also had a high accumulation of trivalent iron and magnetic nanoparticles in the cytoplasm, indicating macrophages treated with *Mms6* mRNA-PS/LNPs acquired the same enhanced abilities of iron uptake and storage as those treated with *Mms6* mRNA-LNPs (Fig. 7, E and F).

The tissue- or cell-targeted properties of mRNA loaded-PS/LNPs were further examined in vivo in SCI mice. After intravenous injection of FLuc mRNA-PS/LNPs, luminescent signals in the liver were way much lower in FLuc mRNA-PS/LNP–treated SCI mice compared with the FLuc mRNA-LNP group (fig. S8, A and B). However, luminescent signals in the injured spinal cord were extremely high, with a peak of about threefold higher than that of the FLuc mRNA-LNP group (fig. S8, A and B). Flow cytometry

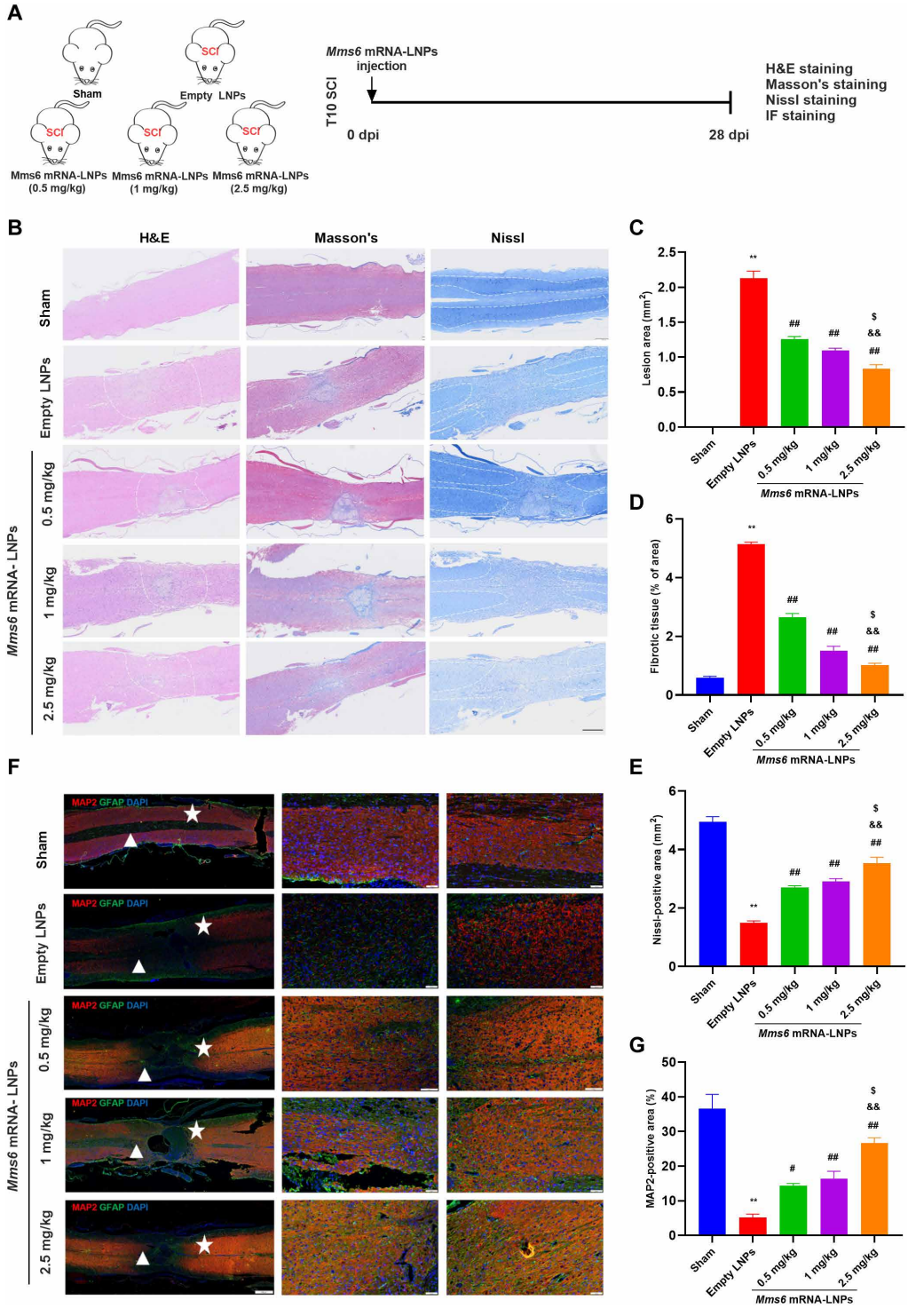

Fig. 4. Intravenous injection of *Mms6* mRNA-LNPs enhanced morphological repair in traumatic SCI mice. (**A**) Schematics of the experimental workflow. SCI mice were received a single injection of *Mms6* mRNA-LNPs. IF, immunofluorescence. (**B**) Representative images of hematoxylin and eosin (H&E), Masson's trichrome, and Nissl staining. Scale bar, 500 μm. Masson's trichrome staining shows scar tissue by staining collagen fibers in blue color. Nissl staining shows the neuronal cell bodies (deep blue). (**C** to **E**) Statistical analysis for H&E staining, Masson's trichrome staining, and Nissl staining ($n = 4$ to 6 mice per group). $^{**}P < 0.01$ versus Sham group; $^{\#\#}P < 0.01$ versus empty LNP group; $^{\&\&}P < 0.01$ versus *Mms6* mRNA-LNP (0.5 mg/kg) group; $^{\$}P < 0.05$ versus *Mms6* mRNA-LNP (1 mg/kg) group. (**F**) Representative images of microtubule-associated protein 2 (MAP2) immunofluorescence staining. Neurons were stained with MAP2 (red). Astrocytes were stained with GFAP (green). Cell nuclei were stained with DAPI (blue). Scale bar, 200 μm. The middle and right panels are magnified views of the star and triangle areas, respectively (scale bars, 50 μm). (**G**) Statistical analysis for percentage of MAP2 positive area ($n = 3$ to 6 mice per group). $^{**}P < 0.01$ versus Sham group; $^{\#}P < 0.05$ versus empty LNP group; $^{\&\&}P < 0.01$ versus *Mms6* mRNA-LNP (0.5 mg/kg) group; $^{\$}P < 0.05$ versus *Mms6* mRNA-LNP (1 mg/kg) group.

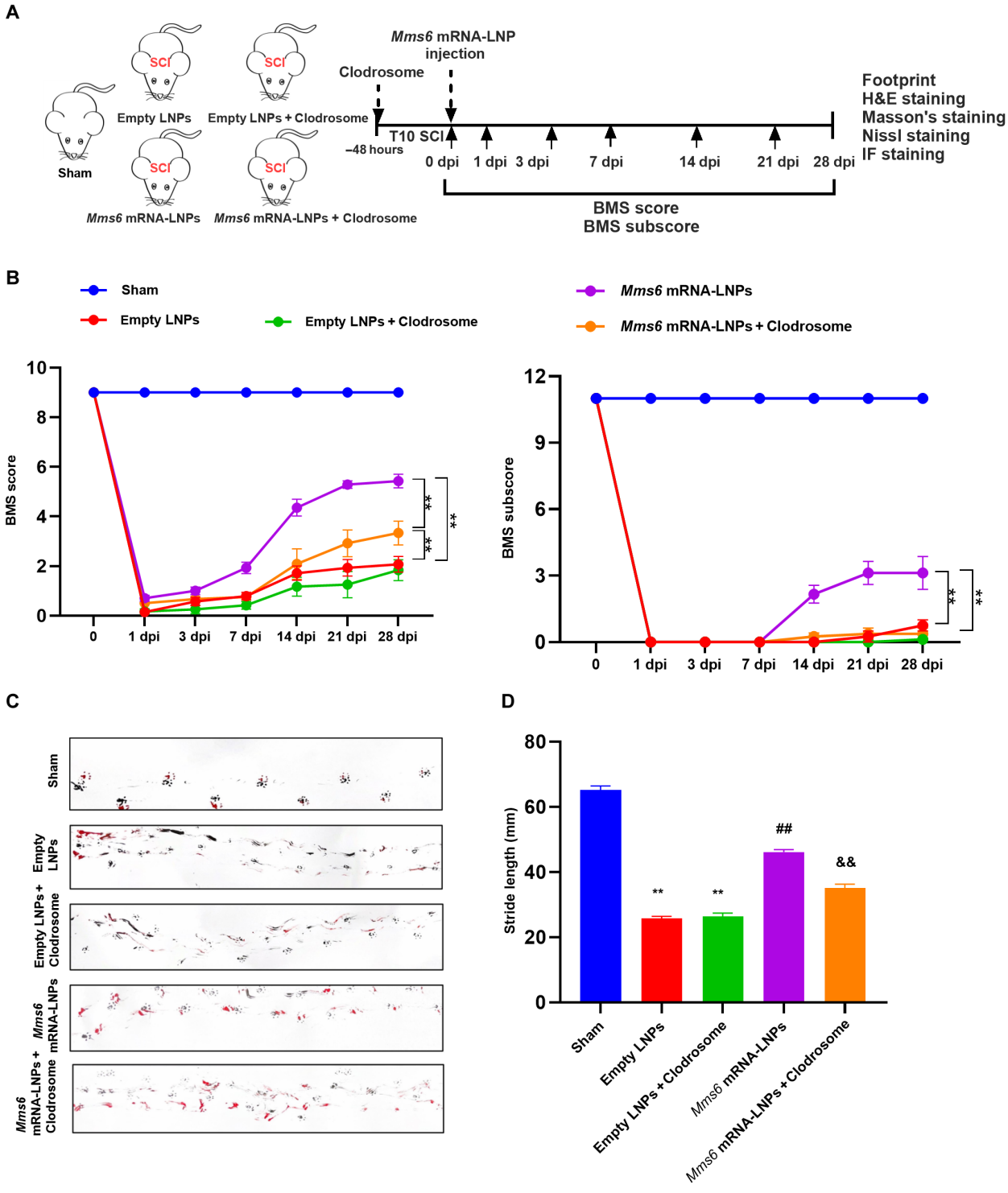

Fig. 5. Depletion of macrophages abolished *Mms6* mRNA-LNP–induced promotion of functional recovery after SCI. (**A**) Schematics of the experimental workflow. (**B**) BMS scores and subscores were assessed after SCI ($n = 6$ mice per group). $^{**}P < 0.01$. (**C**) Representative footprint images at 28 dpi of SCI. The forelimbs and hindlimbs were painted black and red, respectively. (**D**) Evaluation of stride length using footprint images ($n = 6$ mice per group). $^{**}P < 0.01$ versus Sham group; $^{\#\#}P < 0.01$ versus empty LNP group; $^{\&\&}P < 0.01$ versus *Mms6* mRNA-LNP group. dpi, days post-injury.

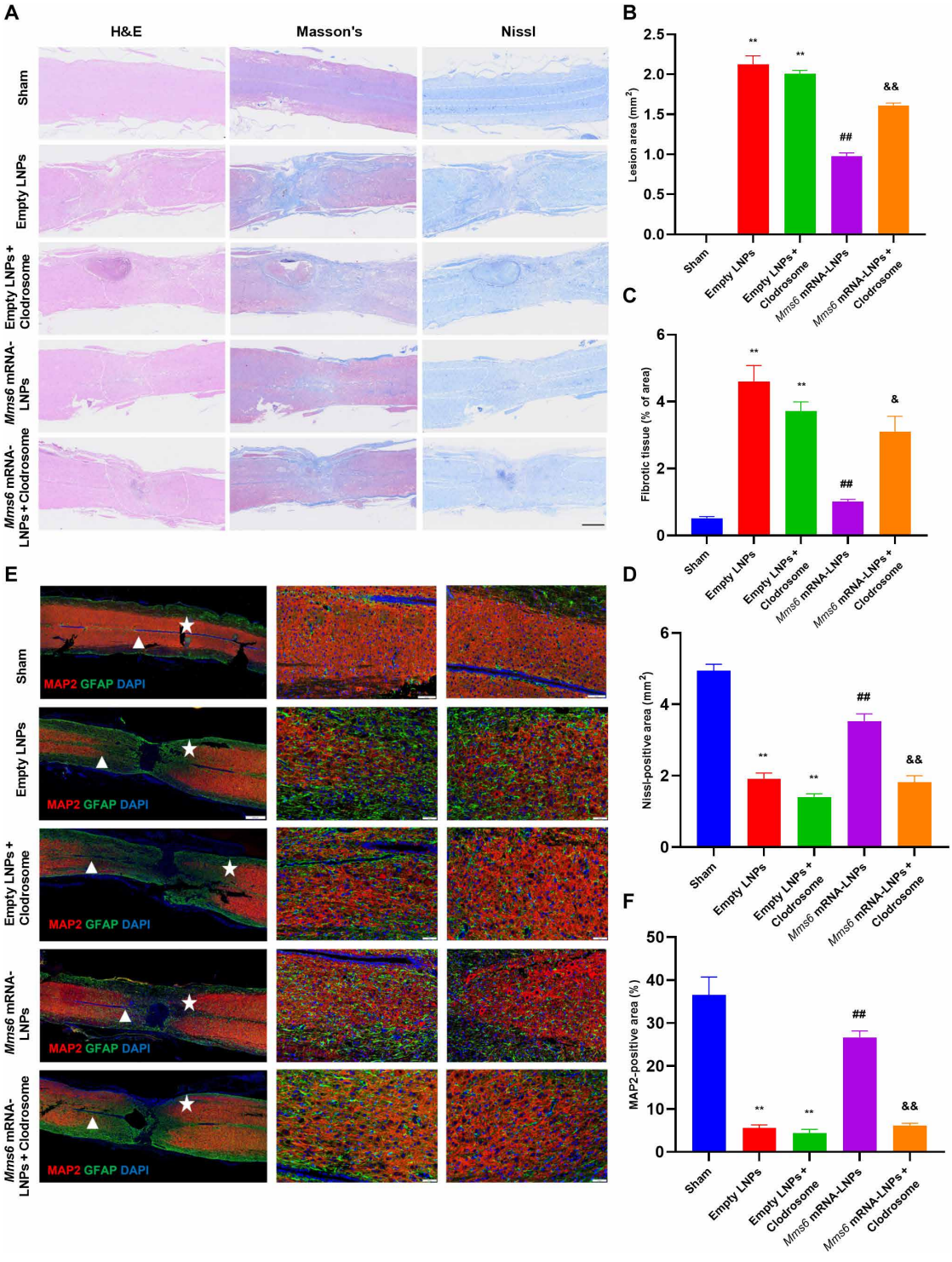

Fig. 6. Depletion of macrophages abolished *Mms6* mRNA-LNP–induced promotion of morphological repair after SCI. (**A**) Representative images of H&E staining, Masson's trichrome staining, and Nissl staining. Scale bar, 500 μm. (**B** to **D**) Statistical analysis for H&E staining, Masson's trichrome staining, and Nissl staining ($n = 4$ to 6 mice per group). $^{**}P < 0.01$ versus Sham group; $^{\#\#}P < 0.01$ versus empty LNP group; $^{\&}P < 0.05$ and $^{\&\&}P < 0.01$ versus *Mms6* mRNA-LNP group. (**E**) Representative fluorescence images of MAP2 staining. Neurons were stained with MAP2 (red). Cell nuclei were stained with DAPI (blue). Astrocytes were stained with GFAP (green). Scale bar, 200 μm. The middle and right panels are magnified views of the triangle and asterisk areas, respectively (scale bars, 50 μm). (**F**) Statistical analysis for percentage of MAP2 positive area ($n = 4$ to 6 mice per group). $^{**}P < 0.01$ versus Sham group; $^{\#\#}P < 0.01$ versus empty LNP group; $^{\&\&}P < 0.01$ versus *Mms6* mRNA-LNP group.

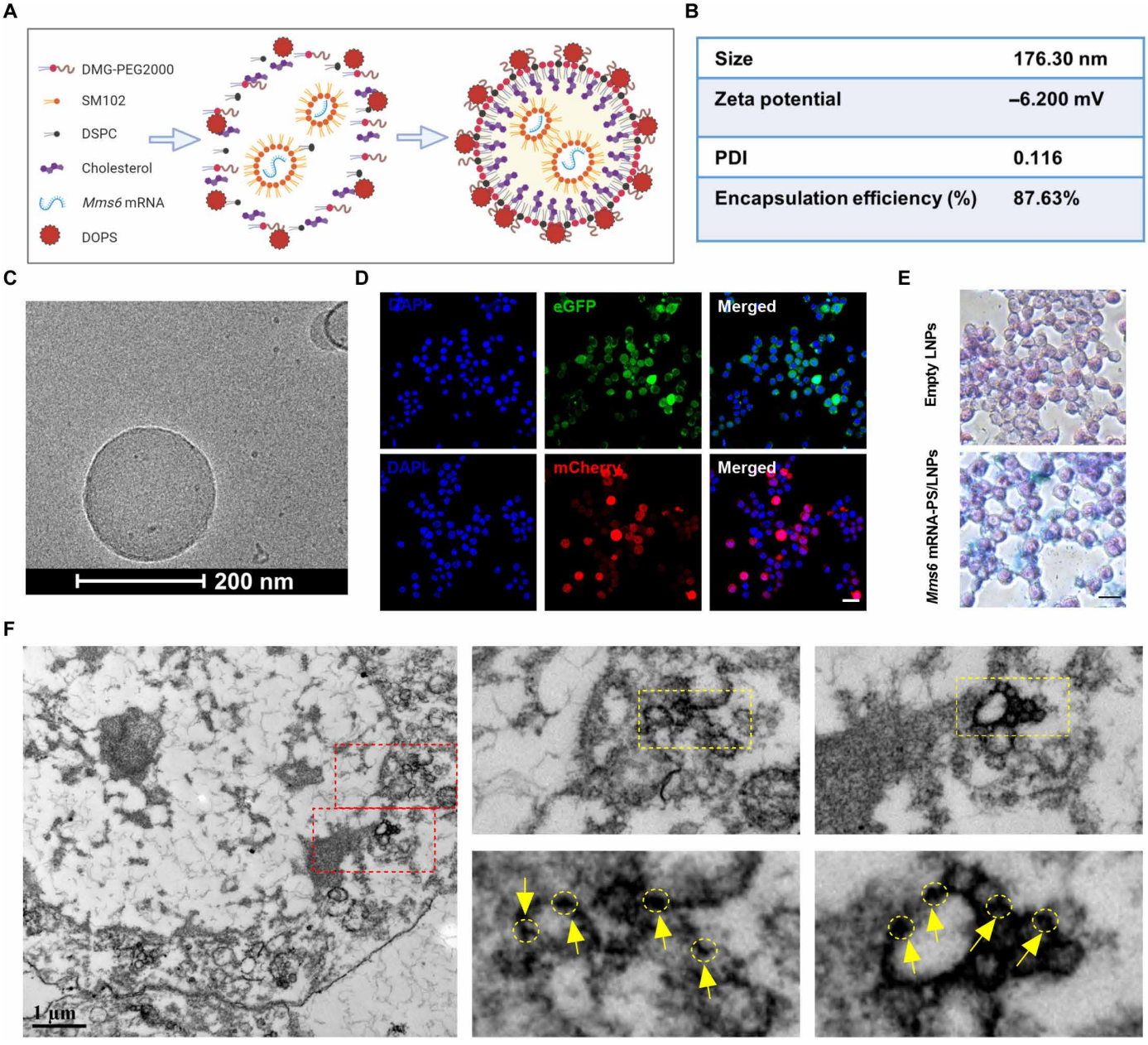

Fig. 7. Characteristics of PS/LNPs containing *Mms6* mRNA. (**A**) Schematic of *Mms6* mRNA-PS/LNP formulation. SM102, an ionizable lipid crucial for forming stable lipid nanoparticles and facilitating endosomal escape from the encapsulated material; DSPC, a phospholipid that helps enhance nanoparticle stability and delivery; cholesterol, allows the outer lipid bilayer of LNPs to maintain integrity and rigidity; DMG-PEG2000, a PEG-lipid that enhances nanoparticle stability and prolongs circulation time by reducing aggregation and immune recognition. 1,2-Dioleoyl-*sn*-glycero-3-phospho-L-serine (DOPS), a negatively charged phospholipid for modulating surface charge of LNPs and facilitating LNPs being recognized by cells such as macrophages; *Mms6* mRNA, encapsulated mRNA encoding the MMS6 protein, which plays a key role in anti-ferroptosis. (**B**) Measurement of particle size, zeta potential, PDI, and encapsulation efficiency of *Mms6* mRNA-PS/LNPs. (**C**) Representative cryo-EM images of *Mms6* mRNA-PS/LNPs. (**D**) Representative eGFP fluorescence (green)–labeled or mCherry fluorescence (red)–labeled *Mms6* mRNA-PS/LNPs in macrophages. Cell nuclei were stained with DAPI (blue). Scale bar, 40 μm. (**E**) Prussian blue stain for detecting storage form of ferric iron in macrophages. Scale bar, 50 μm. (**F**) Representative transmission electron microscopy images of magnetic nanoparticles in *Mms6* mRNA-PS/LNPs transfected macrophages. Scale bar, 1 μm.

data showed that injection of *Mms6*-eGFP mRNA-PS/LNPs did not change the number of total Mφ and their subtypes (M1φ and M2φ) in the injured spinal cord (fig. S8C). Treatment of *Mms6*-eGFP mRNA-PS/LNPs caused a higher transfection efficiency in total macrophages within the injured spinal cord than that of the *Mms6*-eGFP mRNA-LNP administration group (19.03 ± 5.212% versus 5.447 ± 0.189%, $P < 0.01$; fig. S8D). However, the transfection efficiency between M1- and M2-type macrophages in the injured spinal cord had no significant difference (fig. S8D). These results suggested that PS/LNPs could effectively enhance the mRNA delivery to the injured spinal cord, especially preferentially targeted macrophages.

Treatment with *Mms6* mRNA-containing PS/LNPs ameliorated structural abnormalities and motor dysfunction after SCI

Compared with mice treated with *Mms6* mRNA-LNPs, SCI mice administrated with PS/LNPs containing *Mms6* mRNA had better motor functional recovery (Fig. 8, B to E). The lesion area and fibrotic area were smaller, and neuronal survival rate and nerve fiber repair were higher in the injured spinal cord of *Mms6* mRNA-PS/LNP–treated mice than those in *Mms6* mRNA-LNP–treated mice (Fig. 9, A to F). These data suggested that mRNA-loaded PS/LNPs, which had more effective mRNA delivery–targeted macrophages, could strengthen the effect of the *Mms6* mRNA-loaded LNP delivery system on improvement in functional recovery and morphology repair in SCI mice.

DISCUSSION

Because of the hostile microenvironment that develops in the initial stage of traumatic SCI, achieving better functional recovery and morphological repair remains a substantial challenge in the treatment of SCI (*25*). This microenvironment in the injured spinal cord is characterized by hyperinflammation, higher dead cells, and widespread scarring, which impedes the natural self-repair process and weakens the effectiveness of therapeutic interventions (*26*–*28*). The MMS6 protein has been known for its potential anti-ferroptosis property and its ability to enhance the phagocytic functions of macrophages (*9*), and the latter is a pivotal type of immune system cells involved in the early recovery process after SCI (*29*). In the present study, PS-modified LNPs were leveraged to targeted-deliver *Mms6* mRNA to the macrophages at the injury site of SCI, therefore dodging the risk raised by conventional cell transplantation techniques. Meanwhile, the potential therapeutic effect of this approach in protecting against SCI and promoting locomotor functional recovery has also been confirmed.

Our previous study has demonstrated that transplantation of *Mms6* mRNA-modified macrophages has a protective effect in SCI mice (*9*). However, macrophage transplantation involves complex procedures and might cause potential immune reactions. LNP-based mRNA delivery has been recently reported as a promising alternative to overcome the above risk induced by cell-based therapy (*30*). By incorporating advanced mRNA stabilization techniques such as modified nucleosides, synthetic capping, extension of poly-A tails, and codon optimization, the therapeutic mRNA could be transported to target cells and efficiently translated into functional proteins there (*31*). During the process, LNPs serve as an effective delivery system due to their ability to shield mRNA from enzymatic degradation, enhance cellular uptake, and facilitate the release of mRNA within the cytoplasm (*32*). LNPs containing mRNA can be administered via various routes, including intravenous, intraperitoneal, subcutaneous, intramuscular, or intradermal injections (*33*). In this study, LNPs containing *Mms6* mRNA were designed and synthesized. In vivo biodistribution studies have shown that LNPs administrated by the intravenous route could more efficiently deliver mRNA to the injured spinal cord than that given through intraperitoneal injection. As soon as *Mms6* mRNA-LNPs entered the systemic circulation, the physicochemical characteristics of these LNPs allowed them to easily pass through the disrupted blood–spinal cord barrier and arrive at the injured spinal cord. Furthermore, evidence in the present study also confirmed that intravenous injection of *Mms6* mRNA-LNPs could promote locomotor function recovery and morphological repair in traumatic SCI mice.

Macrophages have been proven as pivotal immune cells that participate in the self-repair process immediately after SCI due to their outstanding abilities to remove cellular debris, manage the inflammatory process, and secrete some powerful healing factors (*34*, *35*). However, during the process of spinal cord repair, these infiltrating macrophages within the lesion site would also be continuously consumed, leading to a decay in their self-repair capability, and they might even secrete harmful factors to exacerbate damage or impair the self-repair ability of neighboring parenchymal cells (*36*). So, it is important to find strategies that could mainly target the macrophages and enhance their beneficial functions in the SCI treatment. The results of this study have demonstrated that *Mms6* mRNA-LNPs could enhance the anti-ferroptosis ability of macrophages in both in vivo SCI mice and in vitro hypoxic-mimic conditions. Cellular uptake assay also demonstrated that the uptake of mRNA-loaded LNPs was preferential in microglia/macrophages and neurons. LNPs are easily taken up by cells due to their outer lipid bilayer (*37*). Some studies have indicated that neurons internalize LNPs in a manner distinct from other cells. It has been reported that LNPs might be able to pass through the blood–spinal cord barrier and then be retrogradely transported from the damaged axon terminal to the cell body of neurons (*38*). In the present study, the results also revealed that injection of *Mms6* mRNA-loaded LNPs increased phagocytosis activity of macrophages in the injured spinal cord, but the enhanced internalization of *Mms6* mRNA-loaded LNPs in macrophage did not influence the M1 and M2 polarization. In addition, depletion of macrophages abolished *Mms6* mRNA-LNP–induced promotion of morphological repair and functional recovery after SCI. These results clarified that the protective effects of *Mms6* mRNA-LNPs on SCI mice were substantially dependent on the efficient mRNA delivery of LNPs to macrophages in the injured spinal cord and their enhanced anti-ferroptosis ability.

Although LNPs could deliver mRNA to the injured spinal cord, our results showed that LNPs were mainly accumulated in the liver after being intravenously administrated. Alterations of LNP surface composition might be a great way to reduce their massive uptake by hepatocytes or other cells in the liver. Some studies have found that larger LNPs would lead to less liver uptake (*39*). The PS/LNPs synthesized in the present study were 176.3 nm, which were larger than LNPs. The results also confirmed that PS/LNPs had a much lower accumulation in the liver after being injected than that of LNPs. Our study showed that PS/LNPs did not increase the number of macrophages in the injured spinal cord but enhanced the percentage of mRNA delivery to macrophages. This was consistent with the results that *Mms6* mRNA-PS/LNPs could strengthen the effect of the *Mms6* mRNA-loaded LNP delivery system on improvement in functional recovery and morphology repair in SCI mice.

In summary, our results demonstrated that PS/LNPs loaded with *Mms6* mRNA could effectively target macrophages in the injured spinal cord and promote morphology repair and motor functional recovery via inhibiting macrophage ferroptosis in the injury site (Fig. 10). One benefit of this approach is that it enables direct delivery of mRNA to endogenous cells within the body, therefore potentially eliminating the need for traditional cell transplantation and enhancing the inherent repair mechanisms following SCI. The other favor is that this kind of macrophage-targeted mRNA delivery could minimize the potential adverse effect induced by nonspecific cellular uptake of mRNA. Such PS-modified LNP delivery systems might be promising to help translate some great biomedical achievements into authentic clinical practice in a variety of central nervous system diseases.

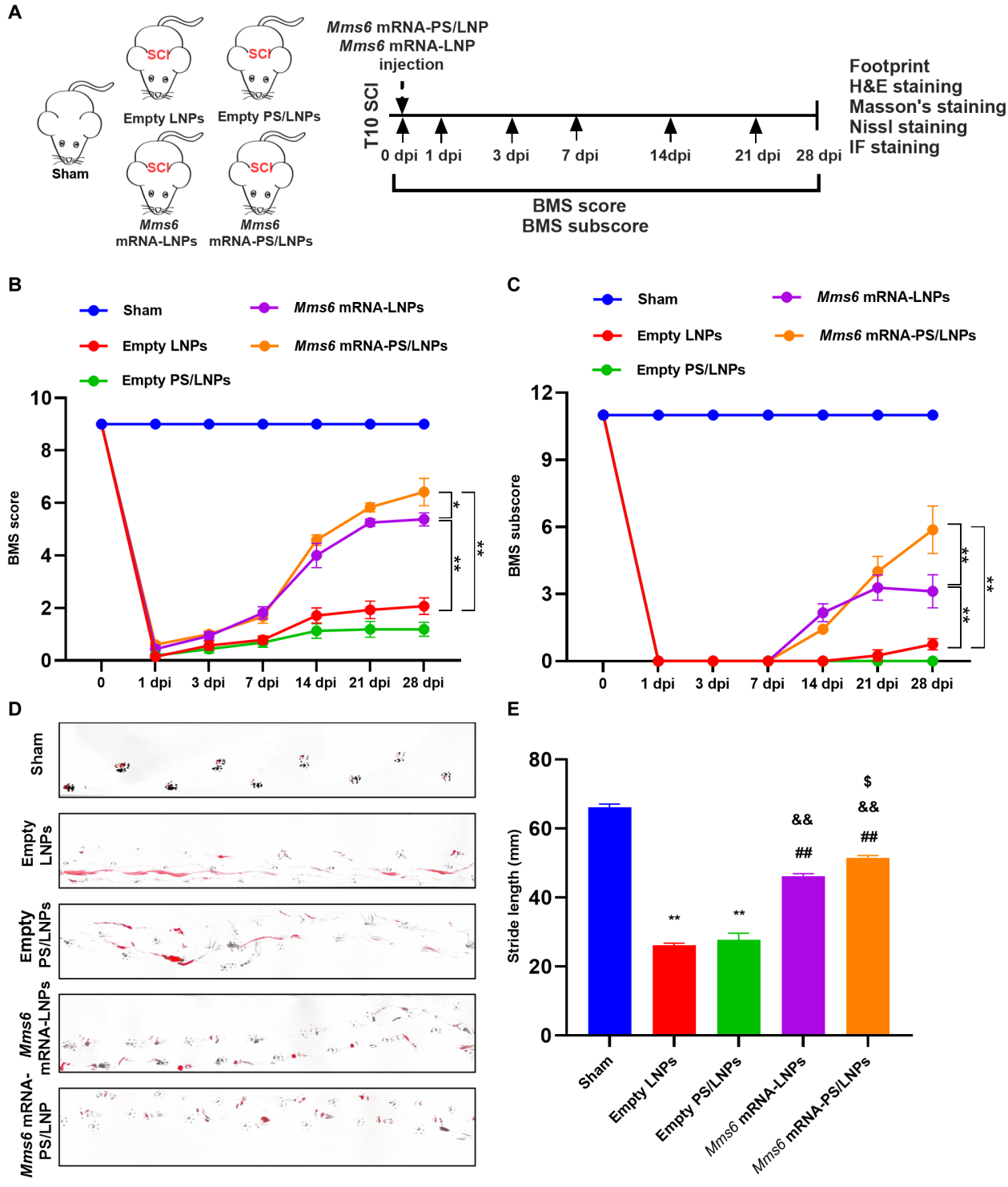

Fig. 8. Treatment with *Mms6* mRNA-containing PS/LNPs ameliorated motor dysfunction after SCI. (**A**) Schematics of the experimental workflow. (**B** and **C**) BMS scores and subscores were assessed after SCI ($n = 6$ mice per group). *$P < 0.05$ and **$P < 0.01$. (**D**) Representative footprint images at 28 dpi of SCI. The forelimbs and hindlimbs were painted black and red, respectively. (**E**) Evaluation of stride length using footprint images ($n = 6$ mice per group). **$P < 0.01$ versus Sham group; ##$P < 0.01$ versus empty LNP group; &&$P < 0.01$ versus empty PS/LNP group; \$$P < 0.05$ versus *Mms6* mRNA-LNP group. dpi, days post-injury.

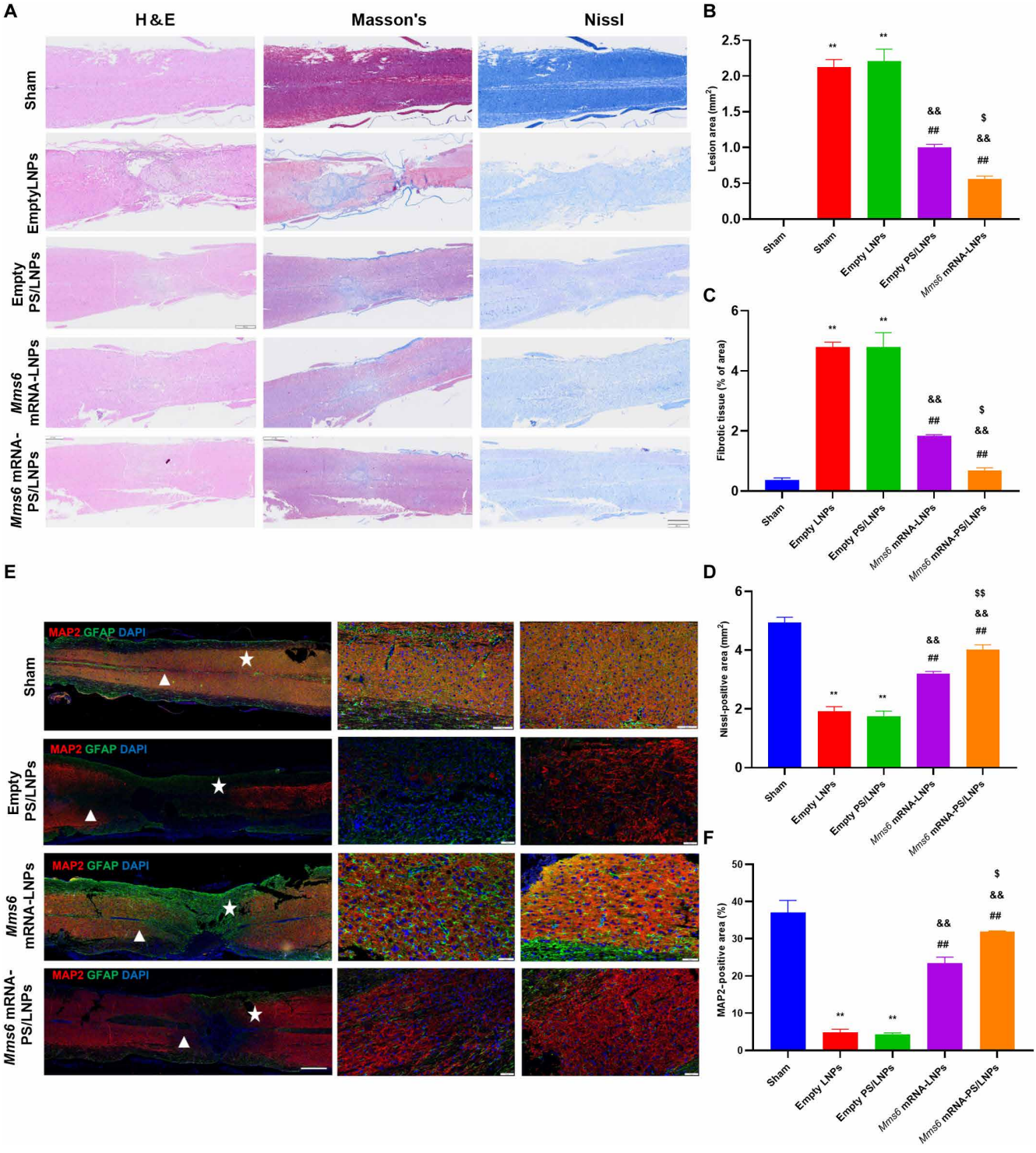

Fig. 9. Treatment with *Mms6* mRNA-containing PS/LNPs ameliorated structural abnormalities after SCI. (**A**) Representative images of H&E staining, Masson's trichrome staining, and Nissl staining. Scale bar, 500 μm. (**B** to **D**) Statistical analysis for H&E staining, Masson's trichrome staining, and Nissl staining ($n = 4$ to 6 mice per group). $^{**}P < 0.01$ versus sham group; $^{\#\#}P < 0.01$ versus empty LNP group; $^{\&\&}P < 0.01$ versus empty PS/LNP group; $\$P < 0.05$ and $\$\$P < 0.01$ versus *Mms6* mRNA-LNP group. (**E**) Representative fluorescence images of MAP2 staining. For representative fluorescence images corresponding to empty LNPs, please refer to the second row of Fig. 4F. Neurons were stained with MAP2 (red). Cell nuclei were stained with DAPI (blue). Astrocytes were stained with GFAP (green). Scale bar, 200 μm. The middle and right panels are magnified views of the triangle and asterisk areas, respectively (scale bars, 50 μm). (**F**) Statistical analysis for percentage of MAP2 positive area ($n = 4$ to 6 mice per group). $^{**}P < 0.01$ versus sham group; $^{\#\#}P < 0.01$ versus empty LNP group; $^{\&\&}P < 0.01$ versus empty PS/LNP group; $\$\$P < 0.01$ versus *Mms6* mRNA-LNP group.

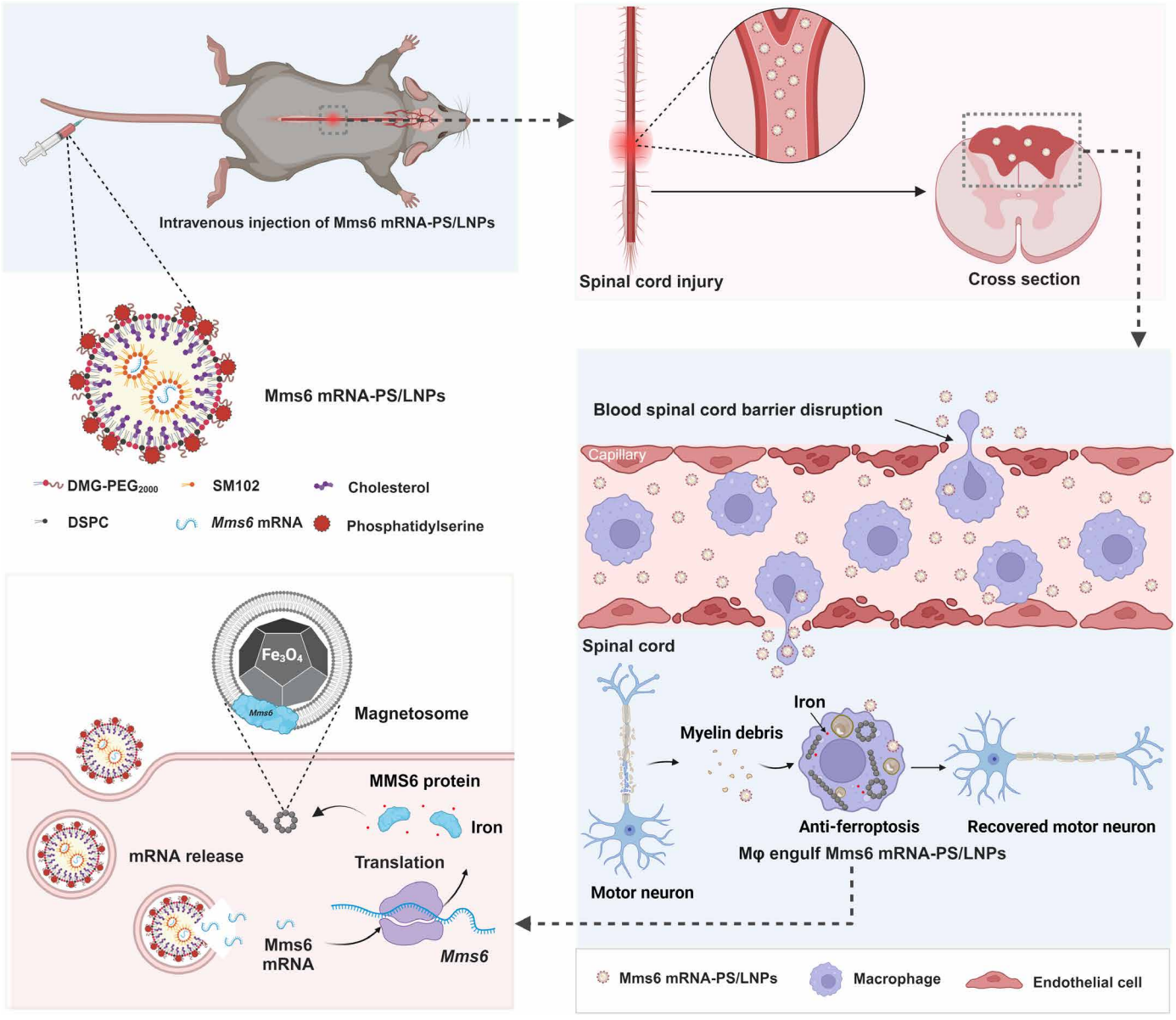

Fig. 10. Macrophage-targeted *Mms6* mRNA-lipid nanoparticles (*Mms6* mRNA-PS/LNPs) promote spinal cord repair and motor function recovery (created with BioRender.com). Intravenous administration of *Mms6* mRNA-PS/LNPs efficiently delivers *Mms6* mRNA to lesion-associated macrophages in the injured spinal cord. This enhances macrophage resistance to ferroptosis, reduces scar formation, promotes neuronal survival, facilitates nerve fiber repair, and notably restores motor function. The therapeutic potential of this strategy was validated in a mouse model of traumatic spinal cord injury, underscoring its promise for spinal cord repair and functional recovery.

Although PS modification of LNPs decreased their accumulation in the liver, many of these LNPs were still taken up in the spleen. Therefore, it is necessary to further explore and search for more specific membrane molecules that can be recognized uniquely by macrophages, so that *Mms6* mRNA-loaded LNPs could more precisely target macrophages. Moreover, further optimizing the size, charge, and other characteristics of LNPs is also needed to improve their ability to cross physiological barriers, facilitate cellular internalization and endosomal escape, and enhance their therapeutic efficacy.

MATERIALS AND METHODS

Formulation and characterization of LNPs and PS/LNPs

LNPs and PS/LNPs were formulated by microfluidic mixing using a syringe pump to combine the ethanol and aqueous phases at a volume ratio of 1:3. For LNPs, the molar ratio of lipids [SM102:1,2-distearoyl-*sn*-glycero-3-phosphocholine (DSPC):cholesterol:1,2-dimyristoyl-rac-glycero-3-methoxypolyethylene glycol-2000) (DMG-PEG2000)] was 50:10:38.5:1.5, with a mass ratio of ionizable lipid SM102 to mRNA of 6:1. For PS/LNPs, the molar ratio of lipids (SM102:DSPC:cholesterol:DMG-PEG2000:1,2-dioleoyl-*sn*-glycero-

3-phospho-L-serine) was 50:10:38.5:1.5:5, also with a mass ratio of SM102 to mRNA of 6:1. The aqueous phase was prepared in 50 mM citrate buffer (pH 4.0) with linear mRNA (APExBIO, USA). LNPs and PS/LNPs were dialyzed overnight in PBS at 4°C using Slide-A-Lyzer MINI Dialysis Devices with molecular weight cutoff (MWCO) of 20 KDa (Thermo Fisher Scientific). After dialysis, LNPs were sterilized using 0.22-μm filters and concentrated using Amicon Ultra-15 centrifugal filter units with a 10-kDa membrane cutoff at 4000 rpm and 4°C. Purified LNPs were stored at 4°C and used within 7 days.

The size of LNPs encapsulating eGFP mRNA (APExBIO, USA) was characterized using dynamic light scattering with a Nano-ZS Zetasizer (Malvern, USA). Zeta potential was measured using electrophoretic light scattering. The morphology of LNP formulations encapsulating eGFP mRNA was observed under cryo-EM. Encapsulation efficiency (EE%) was assessed using a QuantiFluor assay (Promega, USA) to quantify the amount of mRNA in the sample.

Cell culture and treatments

RAW264.7 mouse macrophages were purchased from the Cell Bank of the Chinese Academy of Sciences (Shanghai, China) and cultured in Dulbecco's modified Eagle's medium (DMEM; Gibco) supplemented with 10% fetal bovine serum (FBS) and 1% penicillin-streptomycin at 37°C in a 5% CO_2 incubator. *Mms6* mRNA (10 μg) was loaded in LNPs or PS/LNPs as previously described (*40*, *41*), and LNPs or PS/LNPs containing 100 ng of mRNA were transfected into 10,000 cells. For detection of the anti-ferroptosis ability, the cells were challenged with $CoCl_2$ (200 μM, a hypoxia-mimetic agent) or ferrostatin-1 (1 μM, a ferroptosis inhibitor) for 24 hours.

NSC-34 cells were cultured in DMEM containing 10% FBS and 1% penicillin-streptomycin in a 5% CO_2 incubator at 37°C. Macrophages, transfected with either *Mms6*-loaded LNPs or empty LNPs, were placed in the upper chamber of a coculture system equipped with a 0.4-μm porous membrane (Corning, USA), while NSC-34 cells were seeded in the lower chamber. Following 12-hour incubation in a serum-free medium, macrophages and NSC-34 cells within the coculture setup were exposed to 400 μM $CoCl_2$ for 24 hours. NSC-34 cells were then harvested and subjected to 4′,6-diamidino-2-phenylindole (DAPI) staining for further examination.

Transfection efficiency of LNPs or PS/LNPs in the cultured macrophage

To evaluate the transfection efficiency of LNPs or PS/LNPs in the cultured macrophages, LNPs or PS/LNPs carrying *Mms6-mCherry* mRNA or *Mms6-eGFP* mRNA were added into the medium of cultured macrophages. After 8 hours of incubation, the culture medium was removed. Then, cells were washed with PBS and stained with DAPI for 5 min to visualize cell nuclei. Transfection efficiency was evaluated using fluorescence images of eGFP or mCherry under a confocal laser microscope (Olympus FV3000, Japan).

Prussian blue staining

After different treatments, cells were incubated with a medium containing ferric quinate (34 μM) for 24 hours (*9*). After removing the medium, the cells were fixed with 4% paraformaldehyde for 20 min and washed thrice with PBS. They were then incubated with Perl's reagent (1:1 hydrochloric acid and potassium ferrocyanide) for 30 min, washed with PBS three times, counterstained with 0.02% neutral red for 10 s, and observed under an inverted microscope (Olympus BX61, Japan).

Transmission electron microscopy

The accumulation of magnetic bio-nanoparticles in macrophages was detected using transmission electron microscopy. Macrophages, transfected with *Mms6* mRNA-LNPs or *Mms6* mRNA-PS/LNPs, were treated with ferric quinate (34 μM) for 24 hours and then washed three times with PBS. Following treatment, the cells were fixed with 2.5% glutaraldehyde and 1% osmium tetroxide, gradient dehydrated, and embedded in resin. Sections were then prepared and transferred to copper grids. Last, the samples were observed under transmission electron microscopy.

Animals

Female C57BL/6 mice (8 to 12 weeks, 20 to 25 g) were obtained from the Laboratory Animal Center at Zhejiang University. The mice were housed in a 12-hour/12-hour light-dark cycle, with ad libitum access to food and water. All experiments were conducted in compliance with the Guide for the Care and Use of Laboratory Animals and were approved by the Experimental Animal Ethics Committee of Zhejiang University (no. ZJU20220087).

SCI model and treatment

A mouse model of SCI was established as previously described (*9*). Briefly, mice were anesthetized with 2% sevoflurane and 40% oxygen. A laminectomy was performed to expose the T_{10} spinal cord. Then, a 5-g weight was dropped from a height of 20 mm to induce T_{10} moderate contusion. Mice of the Sham group received only laminectomy. The bladder of SCI mice was manually emptied at least twice a day until reflexive function was observed. In the LNPs or PS/LNPs treated mice, LNPs or PS/LNPs containing mRNA (*eGFP* mRNA or *Mms6* mRNA) in 200 μl of PBS were injected into animals immediately after SCI. For macrophage-depletion experiments, mice were pretreated with 200 μl of Clodrosome (5 mg/ml) via intravenous injections (*21*).

Analysis of in vivo biodistribution of LNPs or PS/LNPs

C57BL/6J mice were administered LNPs or PS/LNPs containing firefly luciferase (FLuc) mRNA (MedChemExpress, Shanghai, China) via intravenous or intraperitoneal injection at a dose of 0.5 mg/kg. At 3, 6, 9, 12, 24, 48, 72, 96, and 120 hours postinjection, the distribution of LNPs or PS/LNPs was detected using the bioluminescence imaging technique by an IVIS Spectrum imaging system (Caliper Life Sciences, Waltham, MA, USA). Briefly, D-luciferin sodium salt (MedChemExpress, Shanghai, China) (150 mg/kg in PBS), a substrate of the enzyme FLuc, was injected intraperitoneally into the mice. Fifteen minutes later, mice were euthanized, and the heart, liver, spleen, lungs, kidneys, and spinal cord were collected. Bioluminescence images (yellow-green light) in these tissues were analyzed using Living Image Software (PerkinElmer).

Analysis for cellular uptake of mRNA-loaded LNPs or PS/LNPs in the injured spinal cord

Mice received intravenous injections of LNPs or PS/LNPs encapsulating *Mms6-eGFP* mRNA or *Mms6-mCherry* mRNA immediately SCI. Nine hours later, the mice were euthanized and perfused with 20 ml of PBS via the left ventricle. Injured spinal cords were isolated and fixed in 4% paraformaldehyde overnight at 4°C. After that, the tissues were washed with cold PBS, dehydrated through graded ethanol (70, 80, 90, and 95%), and embedded in paraffin. Sections with 4-μm

thickness were prepared and stained with antibodies: anti-MAP2 (rabbit; 8707, Cell Signaling Technology; 1:100), anti–glial fibrillary acidic protein (GFAP) (chicken; ab4674, Abcam; 1:200), anti-Iba1 (rabbit; 17198, Cell Signaling Technology; 1:100), anti-CD31 (mouse; 3528, Cell Signaling Technology; 1:1000), and anti-F4/80 (mouse; ab111101, Abcam; 1:100) antibodies and DAPI (catalog no. 425701, BioLegend; 1:500). The sections were scanned using an Olympus VS200 digital section scanner (Olympus, Japan). The colocalization of mCherry and different cells in the injured spinal cord was analyzed.

Flow cytometry analysis

The percentage of infiltrating macrophages (total or subtypes) that phagocytosed mRNA-loaded LNPs or mRNA-loaded PS/LNPs in the injured spinal cord was analyzed. The injured spinal cords of SCI mice were collected, cut into small pieces, and digested in a DMEM buffer containing collagenase/hyaluronidase and deoxyribonuclease I (1 mg/ml) for 30 min at 37°C. The digested cells were filtered through a 70-μm strainer to create single-cell suspensions. After erythrocyte lysis and demyelination, cells were suspended in fluorescence-activated cell sorting (FACS) buffer (2% FBS in PBS) and blocked with anti-CD16/32 antibody for 15 min. The cells were then incubated for 30 min with fluorescent-conjugated antibodies: CD45-phycoerythrin (catalog no. 157604, BioLegend), F4/80-allophycocyanin (catalog no. 157306, BioLegend), CD11b-FITC (catalog no. 101205, BioLegend), CD86-peridinin-chlorophyll protein-cyanine 7 (catalog no. 159208, BioLegend), and CD206-BV785 (catalog no. 141729, BioLegend). Before analysis, cells were stained with DAPI (catalog no. 425701, BioLegend; 1:500). Macrophages ($F4/80^{+}CD45^{high}$), M1 macrophages ($F4/80^{+}CD45^{high}CD86^{+}$), M2 macrophages ($F4/80^{+}CD45^{high}CD206^{+}$), and microglia ($F4/80^{+}CD45^{low}$) were identified using FACS analysis (*42*). The samples were analyzed using a CytoFLEX LX flow cytometer (Beckman Coulter, USA), and the data were processed with FlowJo software.

Ferrous ion and lipid peroxide assay

Intracellular ferrous ions and lipid peroxides in macrophages were detected using FerroOrange and Liperfluo fluorescent probes, respectively (Dojindo, Shanghai, China). Macrophages, either cultured or isolated from injured spinal cords, were collected. The cells were incubated with FerroOrange or Liperfluo for 30 min. After incubation, the cells were washed and resuspended in 500 μl of PBS. For nucleated cell staining, the samples were stained with DAPI (catalog no. 425701, BioLegend; 1:500) for 5 min at 37°C. The fluorescence intensities of FerroOrange or Liperfluo were then analyzed using a CytoFLEX LX flow cytometer (Beckman Coulter, USA).

Locomotor function assay

The hindlimb movement of mice was evaluated using the BMS scoring system on a grid with 80-cm side length. The BMS score ranges from 0 (complete paralysis) to 9 (normal movement), and the subscore ranges from 0 (no movement) to 11 (normal locomotion). Mice with a BMS score greater than 2 at 1 dpi were excluded from the study (*43*). The stride length of the mice was assessed using footprint analysis. The forelimbs and hindlimbs were painted with black and red ink, respectively. Then, the mice were placed on white paper (70 mm by 120 mm) and allowed to walk freely. The stride length was determined by measuring the distance between successive steps of the same hindlimbs.

H&E, Masson's trichrome, and Nissl staining

Tissue samples (spinal cord, heart, liver, spleen, and kidney) were collected from anesthetized mice. The samples were immediately fixed in 4% formaldehyde at room temperature for 24 hours, then dehydrated through a graded series of ethanol solutions (70, 80, 90, and 95%), and embedded in paraffin. The tissues were sectioned into 4-μm-thick slices. Sections of the spinal cord, heart, liver, spleen, and kidney were deparaffinized and stained with H&E for cellular and tissue structure analysis. Additionally, paraffin sections of spinal cords were used for Masson's trichrome and Nissl staining. The slides were photographed and analyzed using the Olympus VS200 Slide Scanner and Olympus OlyVIA v3.2.1 software (Olympus, Japan). In photography and analysis, one slice of each mouse at the injured center was selected, and each group consisted of six slices from six individual mice.

Evaluation of nerve fiber repair using immunofluorescence staining

After different treatments, the injured spinal cords in mice were isolated and fixed in 4% paraformaldehyde overnight at 4°C. Tissues were then dehydrated, embedded, and sliced into 4-μm thickness. Sections were stained with antibodies: anti-MAP2 (rabbit; 8707, Cell Signaling Technology; 1:100), anti-GFAP (chicken; ab4674, Abcam; 1:200), and DAPI (catalog no. 425701, BioLegend; 1:500). The sections were scanned using an Olympus VS200 digital section scanner (Olympus, Japan). Nerve fiber repair in the injured spinal cord was assayed using the percentage of MAP2-positive area.

Macrophage depletion and evaluation of depletion efficiency

Macrophages were depleted by injection of clodronate-contained liposomes (Clodrosome) into mice (Liposoma B.V., Amsterdam, The Netherlands) according to a previously published protocol (*40*). C57BL/6J mice were intravenously injected with 0.2 ml of Clodrosome (5 mg/ml). Mice treated with PBS-containing liposomes without clodronate were used as controls. Flow cytometry and immunohistochemistry were used to assess the efficiency of macrophage depletion in the liver and spleen of mice at 0, 24, 48, and 72 hours after Clodrosome treatment using a mouse anti-F4/80 antibody (ab111101, Abcam; 1:100). Then, the optimal timing of maximum depletion was chosen for further study.

Safety evaluation

C57BL/6 mice underwent intravenous or intraperitoneal injections of LNPs to evaluate their impact on health. Blood samples were collected for biochemical analysis following the experimental procedure. Untreated healthy mice served as the sham group. Liver function was assessed by measuring aspartate aminotransferase, alanine aminotransferase, and alkaline phosphatase, while kidney function was evaluated using blood urea nitrogen levels. These measurements were conducted using a Roche fully automated biochemical analyzer (COBAS C 311).

Statistical analysis

All data are presented as means ± SEM and analyzed using GraphPad Prism software (GraphPad Software Inc.). Statistical differences between two groups were analyzed using a *t* test, while differences among more than two groups were assessed using one-way analysis of variance (ANOVA). BMS scores and subscores were analyzed using two-way ANOVA. A *P* value of less than 0.05 was considered statistically significant.

Supplementary Materials

This PDF file includes:

Figs. S1 to S8
Table S1

REFERENCES AND NOTES

1. C. S. Ahuja, J. R. Wilson, S. Nori, M. R. N. Kotter, C. Druschel, A. Curt, M. G. Fehlings, Traumatic spinal cord injury. *Nat. Rev. Dis. Primers.* **3**, 17018 (2017).
2. X. D. Guo, J. Z. Hu, S. Q. Feng, X. W. Gao, C. K. Sun, Q. Ao, L. Chen, L. K. Chen, P. Zhang, Y. W. Dai, Z. C. Zheng, H. Y. Huang, Chinese Association of Neurorestoratology (Preparatory) and the China Committee of International Association of Neurorestoratology, Clinical neurorestorative treatment guidelines for neurological dysfunctions of sequels from vertebral and spinal cord lesions (CANR 2023 version). *J. Neurorestoratology* **11**, 100070 (2023).
3. H. Y. Huang, J. R. Bach, H. S. Sharma, L. Chen, P. Wu, A. Sarnowska, A. Otom, M. Z. Xue, H. Saberi, X. J. He, Z. Alhawamdeh, D. Kuf, J. Z. Hu, D. Siniscalco, E. O. Alvarez, M. C. Li, P. R. Sanberg, The 2023 yearbook of neurorestoratology. *J. Neurorestoratology* **12**, 100136 (2024).
4. R. C. Sterner, R. M. Sterner, Immune response following traumatic spinal cord injury: Pathophysiology and therapies. *Front. Immunol.* **13**, 1084101 (2022).
5. S. Watanabe, M. Alexander, A. V. Misharin, G. R. S. Budinger, The role of macrophages in the resolution of inflammation. *J. Clin. Invest.* **129**, 2619–2628 (2019).
6. R. Langer, J. Folkman, Polymers for the sustained release of proteins and other macromolecules. *Nature* **263**, 797–800 (1976).
7. M. J. Ostro, D. Giacomoni, D. Lavelle, W. Paxton, S. Dray, Evidence for translation of rabbit globin mRNA after liposome-mediated insertion into a human cell line. *Nature* **274**, 921–923 (1978).
8. K. Ma, S. Xu, T. Tao, J. Qian, Q. Cui, S. U. Rehman, X. Zhu, R. Chen, H. Zhao, C. Wang, Z. Qi, H. Dai, X. Zhang, C. Xie, Y. Lu, H. Wang, J. Wang, Magnetosome-inspired synthesis of soft ferrimagnetic nanoparticles for magnetic tumor targeting. *Proc. Natl. Acad. Sci. U.S.A.* **119**, e2211228119 (2022).
9. C. Y. Fu, X. J. Mao, X. Q. Jin, T. Zuo, M. Z. Zheng, J. Y. Wang, Y. P. Fan, L. T. Xu, J. S. Lou, D. L. Shi, J. J. Zhong, Y. Y. Chen, L. L. Wang, Magnetotactic bacteria-derived *Mms6* Gene helps M2 macrophages to form magnetic bio-nanoparticles to prevent ferroptosis and promote locomotor functional recovery after spinal cord injury in mice. *Adv. Funct. Mater.* **33**, 2305325 (2023).
10. X. Hou, T. Zaks, R. Langer, Y. Dong, Lipid nanoparticles for mRNA delivery. *Nat. Rev. Mater.* **6**, 1078–1094 (2021).
11. L. Y. Jin, J. Li, K. F. Wang, W. W. Xia, Z. Q. Zhu, C. R. Wang, X. F. Li, H. Y. Liu, Blood-spinal cord barrier in spinal cord injury: A review. *J. Neurotrauma* **38**, 1203–1224 (2021).
12. Y. Yang, Y. Fan, H. Zhang, Q. Zhang, Y. Zhao, Z. Xiao, W. Liu, B. Chen, L. Gao, Z. Sun, X. Xue, M. Shu, J. Dai, Small molecules combined with collagen hydrogel direct neurogenesis and migration of neural stem cells after spinal cord injury. *Biomaterials* **269**, 120479 (2021).
13. J. G. Rurik, I. Tombacz, A. Yadegari, P. O. Mendez Fernandez, S. V. Shewale, L. Li, T. Kimura, O. Y. Soliman, T. E. Papp, Y. K. Tam, B. L. Mui, S. M. Albelda, E. Pure, C. H. June, H. Aghajanian, D. Weissman, H. Parhiz, J. A. Epstein, CAR T cells produced in vivo to treat cardiac injury. *Science* **375**, 91–96 (2022).
14. L. Breda, T. E. Papp, M. P. Triebwasser, A. Yadegari, M. T. Fedorky, N. Tanaka, O. Abdulmalik, G. Pavani, Y. Wang, S. A. Grupp, S. T. Chou, H. Ni, B. L. Mui, Y. K. Tam, D. Weissman, S. Rivella, H. Parhiz, In vivo hematopoietic stem cell modification by mRNA delivery. *Science* **381**, 436–443 (2023).
15. J. Nong, P. M. Glassman, V. V. Shuvaev, S. Reyes-Esteves, H. C. Descamps, R. Y. Kiseleva, T. E. Papp, M. G. Alameh, Y. K. Tam, B. L. Mui, S. Omo-Lamai, M. E. Zamora, T. Shuvaeva, E. Arguiri, X. Gong, T. V. Brysgel, A. W. Tan, A. G. Woolfork, A. Weljie, C. A. Thaiss, J. W. Myerson, D. Weissman, S. E. Kasner, H. Parhiz, V. R. Muzykantov, J. S. Brenner, O. A. Marcos-Contreras, Targeting lipid nanoparticles to the blood-brain barrier to ameliorate acute ischemic stroke. *Mol. Ther.* **32**, 1344–1358 (2024).
16. P. A. Leventis, S. Grinstein, The distribution and function of phosphatidylserine in cellular membranes. *Annu. Rev. Biophys.* **39**, 407–427 (2010).
17. M. B. Naeini, V. Bianconi, M. Pirro, A. Sahebkar, The role of phosphatidylserine recognition receptors in multiple biological functions. *Cell. Mol. Biol. Lett.* **25**, 23 (2020).
18. P. Assinck, G. J. Duncan, B. J. Hilton, J. R. Plemel, W. Tetzlaff, Cell transplantation therapy for spinal cord injury. *Nat. Neurosci.* **20**, 637–647 (2017).
19. C. M. Zipser, J. J. Cragg, J. D. Guest, M. G. Fehlings, C. R. Jutzeler, A. J. Anderson, A. Curt, Cell-based and stem-cell-based treatments for spinal cord injury: Evidence from clinical trials. *Lancet Neurol.* **21**, 659–670 (2022).
20. F. Feng, X. Song, Z. Tan, Y. Tu, L. Xiao, P. Xie, Y. Ma, X. Sun, J. Ma, L. Rong, L. He, Cooperative assembly of a designer peptide and silk fibroin into hybrid nanofiber gels for neural regeneration after spinal cord injury. *Sci. Adv.* **9**, eadg0234 (2023).
21. T. H. Choi, R. J. Yoo, J. Y. Park, J. Y. Kim, Y. C. Ann, J. Park, J. S. Kim, K. Kim, Y. J. Shin, Y. J. Lee, K. C. Lee, J. Park, H. Chung, S. H. Seok, H. J. Im, Y. S. Lee, Development of finely tuned liposome nanoplatform for macrophage depletion. *J. Nanobiotechnol.* **22**, 83 (2024).
22. L. Meziani, M. Mondini, B. Petit, A. Boissonnas, V. de Thomas Montpreville, O. Mercier, M. C. Vozenin, E. Deutsch, CSF1R inhibition prevents radiation pulmonary fibrosis by depletion of interstitial macrophages. *Eur. Respir. J.* **51**, 1702120 (2018).
23. K. Segawa, S. Nagata, An apoptotic 'Eat Me' signal: Phosphatidylserine exposure. *Trends Cell Biol.* **25**, 639–650 (2015).
24. R. Rodriguez-Manzanet, R. DeKruyff, V. K. Kuchroo, D. T. Umetsu, The costimulatory role of TIM molecules. *Immunol. Rev.* **229**, 259–270 (2009).
25. B. Fan, Z. Wei, S. Feng, Progression in translational research on spinal cord injury based on microenvironment imbalance. *Bone Res.* **10**, 35 (2022).
26. Y. You, J. Jiang, G. Zheng, Z. Chen, Y. X. Zhu, H. Ma, H. Lin, X. Guo, J. Shi, In situ piezoelectric-catalytic anti-inflammation promotes the rehabilitation of acute spinal cord injury in synergy. *Adv. Mater.* **36**, e2311429 (2024).
27. Y. Xu, Y. Geng, H. Wang, H. Zhang, J. Qi, F. Li, X. Hu, Y. Chen, H. Si, Y. Li, X. Wang, H. Xu, J. Kong, Y. Cai, A. Wu, W. Ni, J. Xiao, K. Zhou, Cyclic helix B peptide alleviates proinflammatory cell death and improves functional recovery after traumatic spinal cord injury. *Redox Biol.* **64**, 102767 (2023).
28. A. Fang, Y. Wang, N. Guan, Y. Zuo, L. Lin, B. Guo, A. Mo, Y. Wu, X. Lin, W. Cai, X. Chen, J. Ye, Z. Abdelrahman, X. Li, H. Zheng, Z. Wu, S. Jin, K. Xu, Y. Huang, X. Gu, B. Yu, X. Wang, Porous microneedle patch with sustained delivery of extracellular vesicles mitigates severe spinal cord injury. *Nat. Commun.* **14**, 4011 (2023).
29. J. Wang, L. Xu, W. Lin, Y. Yao, H. Li, G. Shen, X. Cao, N. He, J. Chen, J. Hu, M. Zheng, X. Song, Y. Ding, Y. Shen, J. Zhong, L. L. Wang, Y. Y. Chen, Y. Zhu, Single-cell transcriptome analysis reveals the immune heterogeneity and the repopulation of microglia by Hif1alpha in mice after spinal cord injury. *Cell Death Dis.* **13**, 432 (2022).
30. Y. R. Na, S. W. Kim, S. H. Seok, A new era of macrophage-based cell therapy. *Exp. Mol. Med.* **55**, 1945–1954 (2023).
31. S. Qin, X. Tang, Y. Chen, K. Chen, N. Fan, W. Xiao, Q. Zheng, G. Li, Y. Teng, M. Wu, X. Song, mRNA-based therapeutics: Powerful and versatile tools to combat diseases. *Signal Transduct. Target. Ther.* **7**, 166 (2022).
32. J. R. Melamed, S. S. Yerneni, M. L. Arral, S. T. LoPresti, N. Chaudhary, A. Sehrawat, H. Muramatsu, M. G. Alameh, N. Pardi, D. Weissman, G. K. Gittes, K. A. Whitehead, Ionizable lipid nanoparticles deliver mRNA to pancreatic beta cells via macrophage-mediated gene transfer. *Sci. Adv.* **9**, eade1444 (2023).
33. N. Pardi, S. Tuyishime, H. Muramatsu, K. Kariko, B. L. Mui, Y. K. Tam, T. D. Madden, M. J. Hope, D. Weissman, Expression kinetics of nucleoside-modified mRNA delivered in lipid nanoparticles to mice by various routes. *J. Control. Release* **217**, 345–351 (2015).
34. X. Freyermuth-Trujillo, J. J. Segura-Uribe, H. Salgado-Ceballos, C. E. Orozco-Barrios, A. Coyoy-Salgado, Inflammation: A target for treatment in spinal cord injury. *Cells* **11**, 2692 (2022).
35. D. M. Mosser, K. Hamidzadeh, R. Goncalves, Macrophages and the maintenance of homeostasis. *Cell. Mol. Immunol.* **18**, 579–587 (2021).
36. X. Hu, W. Xu, Y. Ren, Z. Wang, X. He, R. Huang, B. Ma, J. Zhao, R. Zhu, L. Cheng, Spinal cord injury: Molecular mechanisms and therapeutic interventions. *Signal Transduct. Target. Ther.* **8**, 245 (2023).
37. C. H. Albertsen, J. A. Kulkarni, D. Witzigmann, M. Lind, K. Petersson, J. B. Simonsen, The role of lipid components in lipid nanoparticles for vaccines and gene therapy. *Adv. Drug Deliv. Rev.* **188**, 114416 (2022).
38. T. Fukui, H. Tateno, T. Nakamura, Y. Yamada, Y. Sato, N. Iwasaki, H. Harashima, K. Kadoya, Retrograde axonal transport of liposomes from peripheral tissue to spinal cord and DRGs by optimized phospholipid and CTB modification. *Int. J. Mol. Sci.* **23**, 6661 (2022).
39. J. Di, Z. Du, K. Wu, S. Jin, X. Wang, T. Li, Y. Xu, Biodistribution and non-linear gene expression of mRNA LNPs affected by delivery route and particle size. *Pharm. Res.* **39**, 105–114 (2022).
40. S. Luozhong, Z. F. Yuan, T. Sarmiento, Y. Chen, W. C. Gu, C. McCurdy, W. T. Gao, R. X. Li, S. Wilkens, S. Y. Jiang, Phosphatidylserine lipid nanoparticles promote systemic RNA delivery to secondary lymphoid organs. *Nano Lett.* **22**, 8304–8310 (2022).
41. M. Gomi, Y. Sakurai, M. Sato, H. Tanaka, Y. Miyatake, K. Fujiwara, M. Watanabe, S. Shuto, Y. Nakai, K. Tange, H. Hatakeyama, H. Akita, Delivering mRNA to secondary lymphoid tissues by phosphatidylserine-loaded lipid nanoparticles. *Adv. Healthc. Mater.* **12**, e2202528 (2023).
42. L. de Oliveira Coser, M. T. Comelis, D. E. de Costa Matoso, L. P. Cartarozzi, A. L. R. de Oliveira, Flow cytometry characterization and analysis of glial and immune cells from the spinal cord. *Neuroglia* **5**, 129–144 (2024).
43. D. M. Basso, L. C. Fisher, A. J. Anderson, L. B. Jakeman, D. M. McTigue, P. G. Popovich, Basso Mouse Scale for locomotion detects differences in recovery after spinal cord injury in five common mouse strains. *J. Neurotrauma* **23**, 635–659 (2006).

Acknowledgments: We thank the Bio-ultrastructure Analysis Lab of the Analysis Center of Agrobiology and Environmental Sciences, Zhejiang University, for technical support, with

special thanks to J. Li for assistance with TEM. We also acknowledge the core facilities of Zhejiang University School of Medicine for their technical assistance, especially C. Guo and J. Wang for help with flow cytometry, and Q. Huang for assistance with the Olympus VS200 Slide Scanner. Additionally, we express our gratitude to the Cryo-electron Microscopy Center of Zhejiang University School of Medicine, particularly L. Wu for help with cryo–electron microscopy. Last, we appreciate the technical support provided by the Institute of Life Sciences of Zhejiang University, with special thanks to J. Cheng for assistance with IVIS Spectrum. **Funding:** This study was partly supported by grants from the National Natural Science Foundation of China (grant nos. 82172527 and 81972138), the President's Fund of Tarim University (grant no. TDZKCX202312), and Bingtuan Science and Technology Program (grant no.2023ZD106). **Author contributions:** Conceptualization: C.F., J.Z., Y.C., and L.W. Methodology: C.F., K.J., K.L., X.M., P.L., J.Z., Y.C., and L.W. Investigation: C.F., X.J., K.J., Z.H., J.C., F.Z., X.H., L.S., N.L, Y.C., and L.W. Visualization C.F., L.S., Y.C., and L.W. Funding acquisition: C.F., Y.C., and L.W. Project administration: C.F., X.H., L.S., J.Z., Y.C., and L.W. Supervision: C.F., J.Z., Y.C., and L.W. Writing—original draft: C.F., Y.C., and L.W. Writing—review and editing: C.F., F.Z., J.Z., Y.C., and L.W. **Competing interests:** The authors declare that they have no competing interests. **Data and materials availability:** All data needed to evaluate the conclusions in the paper are present in the paper and/or the Supplementary Materials.

Submitted 3 August 2024
Accepted 21 February 2025
Published 26 March 2025
10.1126/sciadv.ads2295